\$ SUPER

Contents lists available at ScienceDirect

Applications in Energy and Combustion Science

journal homepage: www.sciencedirect.com/journal/applications-in-energy-and-combustion-science





Fate of ilmenite as oxygen carrier during 1 MW_{th} chemical looping gasification of biogenic residues

Paul Dieringer^{a,*}, Falko Marx^a, Florian Lebendig^b, Michael Müller^b, Andrea Di Giuliano^c, Katia Gallucci^c, Jochen Ströhle^a, Bernd Epple^a

- ^a Institute for Energy Systems and Technology (EST), Technical University Darmstadt, Otto-Berndt-Str. 2, 64287 Darmstadt, Germany
- ^b Forschungszentrum Jülich GmbH, Institute for Energy and Climate Research (IEK-2), Wilhelm-Johnen-Straβe, 52428 Julich, Germany
- ^c Department of Industrial and Information Engineering and Economics (DIIIE), University of L'Aquila, Piazzale E. Pontieri 1, Loc. Monteluco di Roio, 67100 L'Aquila, Italy

ARTICLE INFO

Keywords: Chemical looping Gasification Oxygen carrier Pilot scale Fluidized bed Ilmenite Biomass

ABSTRACT

Chemical looping gasification (CLG) is a novel gasification technology, allowing for the efficient conversion of different solid feedstocks (e.g. biogenic residues) into a high-calorific syngas. As in any chemical looping technology, the oxygen carrier (OC), transporting heat and oxygen from the air to the fuel reactor, is crucial in attaining high process efficiencies. To investigate the fate of the OC during CLG in an industrial environment, ilmenite samples, collected during >400 hours of chemical operation in 1 MWth scale using three different biomass feedstocks, were analyzed using different lab techniques. In doing so, changes in OC particle morphology and composition induced by CLG operation were determined. Moreover, the most important physical and chemical characteristics of the utilized OC were measured. The ensuing dataset allowed for an indepth evaluation of the CLG technology in semi-industrial scale in terms of OC lifetime and durability. It was found that in the absence of agglomeration, the cycled OC exhibits an oxygen transport capacity of 2.6 wt.-%, a particle density of 3400 kg/m³ and particle diameters between 60 and 250 µm in steady-state conditions. Moreover, it was found that OC loss via particle attrition determines the lifetime of the OC inside the 1 MWth CLG system. On the other hand, feedstock-related agglomeration, observed during CLG operation with wheat straw, was shown to impede OC circulation between AR and FR and thus prevent efficient CLG operation. In summary, the present study thus not only highlights that generally long-term CLG operation in industry-like conditions is feasible, but also provides important insights into measures to improve OC lifetime and durability inside an industrial chemical looping system, such as an optimization of cyclone efficiency or tailored pre-treatment of the utilized feedstock.

1. Introduction

With the global average temperature increase being predicted to exceed the threshold of $+1.5^{\circ}$ C, within the next four years with great likelihood [1], it is clear that the window for efforts to limit global warming to this critical limit, which was pledged not to be exceeded unilaterally by the world's leaders in the Paris Agreement [2], is closing. Consequently, immediate and unmatched global actions in all sectors are necessary to guarantee the well-being of future generations. One sector for which greenhouse gas (GHG) emissions were not reduced in the past decades [3], despite persistent pledges from industry and politics, is the transport sector. While big advances in electrification of

passenger vehicles were realized in recent years [4], thereby promising a reduction of the future carbon-footprint of personal transport on the earth's atmosphere, alternative approaches are required for other modes of transport (e.g. aviation, heavy transport, shipping) [5]. An auspicious route under consideration for the de-fossilization of those means of transport is the production of 2nd generation biofuels. Here, a promising pathway is the thermochemical conversion of biogenic residues into a high-calorific syngas, before further treatment and fuel synthesis [6,7]. Commonly, this is achieved using oxygen-blown gasifiers, in which the feedstock is partially oxidized yielding a high-calorific syngas [8,9]. A novel gasification pathway allowing for an efficient production of synthesis gas from different solid feedstocks is the chemical looping gasification (CLG) technology. Here, an active bed material, called oxygen

E-mail address: paul.dieringer@est.tu-darmstadt.de (P. Dieringer).

^{*} Corresponding author.

Nomenclature GHG greenhouse gas					
		ILMc	coarse ilmenite		
Latin syn	nbols	ILMf	fine ilmenite		
AJI	attrition index	IWP	industrial wood pellets		
c_p	heat capacity	K1/2/3	campaign 1/2/3		
d_p	particle diameter	LS	loop seal		
h	height	OC	oxygen carrier		
$m_{inv.}$	mass inventory of riser	PFR	pine forest residue		
m_i	mass of species i	PSD	particle size distribution		
\dot{m}_i	mass flow of species i	TGA	thermogravimetric analysis		
P	power	WSP	wheat straw pellets		
p	pressure	SEM	scanning electron microscopy		
$Q_{3,i}$	mass fraction of particles with size i	EDX	energy dispersive X-ray spectroscopy		
R_{OC}	oxygen transport capability	EDXRF	EDX- fluorescence spectroscopy		
T	temperature	XRD	X-ray diffraction		
t	time	- 1			
и	velocity	Indices			
RI	rate index	0	reference state		
\dot{Q}	heat flow	AR	air reactor		
~		bulk	bulk		
Greek sy		circ	circulating		
Δm_i	change in mass of species i	exp	experimental		
Δt	change in time	FA	fly ash		
$ au_{LT,OC}$	OC lifetime	FR	fuel reactor		
η_{Cyc}	cyclone separation efficiency	fines	fines		
ρ	density	norm	normalized		
ω	mass conversion of OC	MU	make-up		
		m	mean		
	ns/abbreviations	mf	minimum fluidization		
AR	air reactor	mb	minimum bubbling		
BA	bottom ash	0	oxygen		
CCS/U	carbon capture & storage/utilization	OC	oxygen carrier		
CFB	circulating fluidized bed reactor	ox	oxidized/oxidation		
CLG	chemical looping gasification	p	particle		
CLC	chemical looping combustion	red	reduced/reduction		
DFBG	dual fluidized bed gasification	ref	reference		
FR	fuel reactor	th	thermal		

carrier (OC), is transferred between two reactors. Its purpose is to transport heat and oxygen from the air reactor (AR) to the fuel reactor (FR), in which the solid feedstock is converted into a high-calorific syngas (see Fig. 1). As the OC provides oxygen for the gasification reactions occurring inside the FR, CLG constitutes an oxygen-driven gasification technology. However, as opposed to conventional oxygen-blown gasifiers, CLG does, not rely on a costly air separation unit, as the oxygen is selectively taken-up from the inlet air inside the AR by the OC. Another inherent characteristic of the CLG technology is that it facilitates an efficient capturing of the CO₂ formed during the autothermal gasification step. For biomass-to-liquid process chains this means that the CO₂ contained in the N₂-free raw syngas is removed in the downstream syngas purification unit, thus allowing for net negative CO₂ emissions of the process chain, in case it is captured (CCS) or utilized (CCU) in subsequent process steps [6,10].

With novel synthesis pathways for carbon-neutral or carbon-negative fuels being in demand globally, research on the CLG technology has experienced a push in recent years. However, so far its investigation was mainly restricted to lab-scale [11–13] or small pilot-scale [14–16] units, thereby leaving a major research gap, i.e. the advancement of the CLG technology to higher technology readiness levels via pilot-scale investigations in an industrially-relevant environment. By modifying an existing modular 1 MW_{th} pilot plant, previously used for carbonate looping [17,18], chemical looping combustion [19,20], and High Temperature Winkler gasification [9,21], for CLG operation [22], the

investigation of the CLG technology in such conditions was facilitated, allowing for in-depth analyses of different phenomena occurring inside a CLG unit in industry-like conditions.

Due to the importance of the OC for chemical looping processes (esp. heat & oxygen transport), one aspect crucial for the up-scaling of the CLG technology is the fate of the OC inside the CLG unit, deciding on process efficiency (e.g. OC activity, material loss) as well as process economics (e.g. material procurement and disposal costs). To cast light onto this subject, early work analyzed the suitability of various OCs in lab scale setups [23]. Generally, ilmenite is considered to be an auspicious OC for chemical looping application, due to its low price, high availability, and advantageous physio-chemical properties (e.g. mechanical rigidity and activity) [24,25]. To investigate the long term effect of chemical looping on ilmenite properties, it was investigated in different lab-scale setups under relevant redox conditions [26-28]. Here, it was found that ilmenite particles undergo characteristic changes during redox cycling, manifesting themselves in an increasing particle porosity, the formation of an iron-rich shell on the particle surface, an overall decrease in their oxygen transport capacity, and a decrease in their attrition resistance. While these findings are universally agreed upon, only limited information on the fate of the OC in real chemical looping setups is available. Generally, this data stems from small lab or pilot plants [11,29-31], giving first insights into the fate of the OC during CLG operation. Apart from confirming general findings made in lab-scale, these studies provide insights into the fate of the OC in real

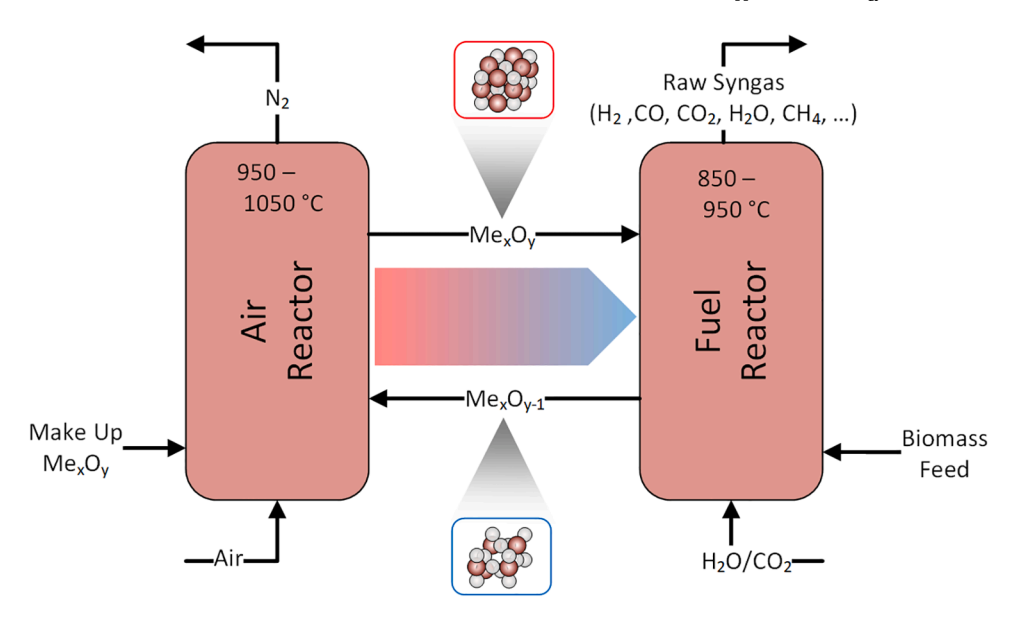


Fig. 1. Schematic illustration of CLG process.

chemical looping systems, with regard to attrition rates, agglomeration behavior, or OC phase composition. However, when striving for reliable information on the performance of OC materials in large-scale setups, the investigation of changes in OC properties occurring during chemical looping operation in an industrially-relevant environment is indispensable.

First and foremost, efficient CLG operation requires sufficiently long oxygen carrier lifetimes, translating in low make-up and material loss rates, which are crucial for operation both technically and economically

[24]. Generally, the OC needs to be replaced due to one (or multiple) of the following reasons [24]:

- Attrition: Due to thermal, chemical, and mechanical strain inside the CLG system, the OC particles in the system can break or abrade leading to a decrease in particle size and ultimately material loss via the cyclone into the downstream filters.
- Agglomeration: In case of thermal (e.g. sintering/melting) or chemical (e.g. ash interactions) influences OC particles can

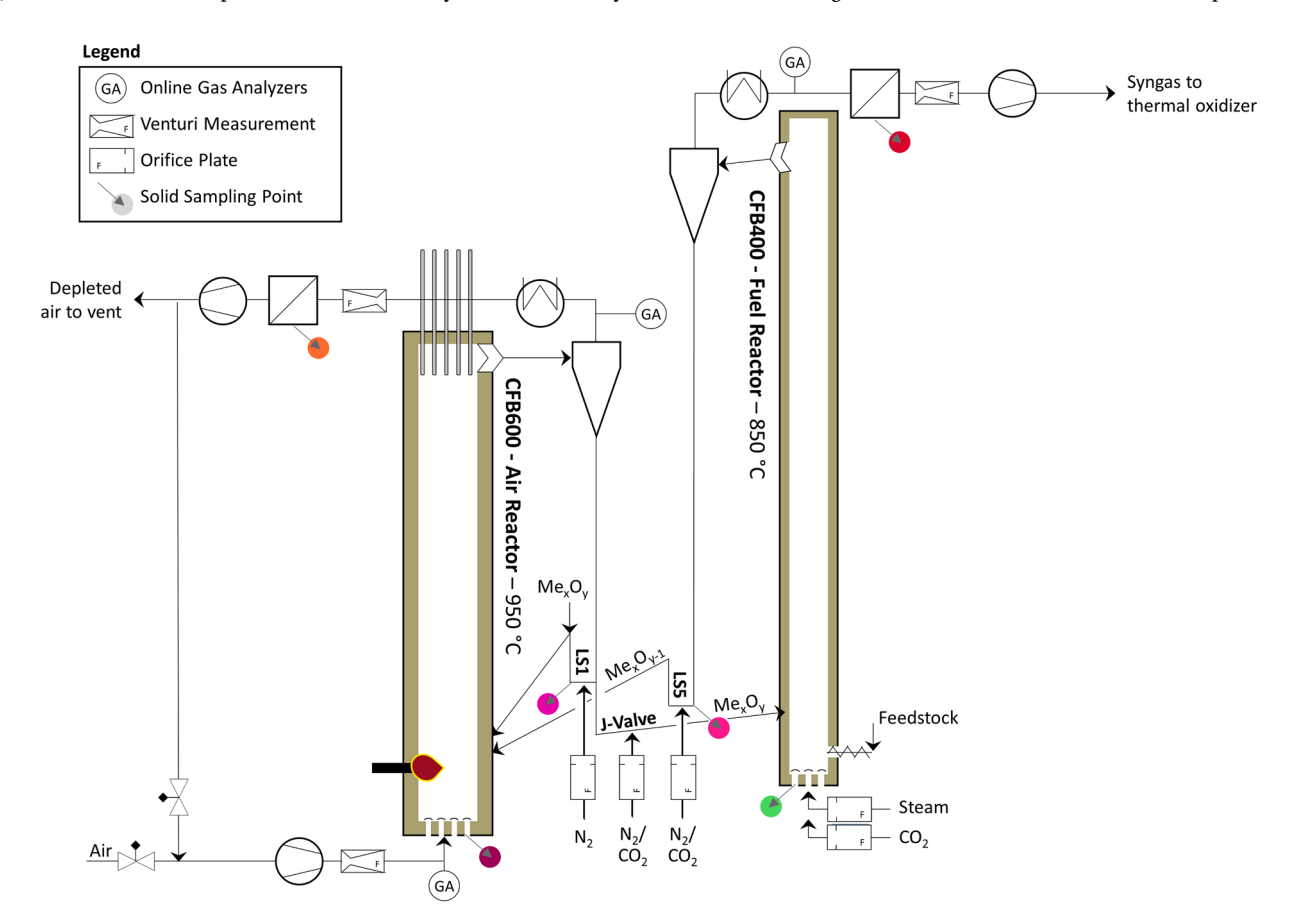


Fig. 2. Simplified flow diagram of the 1 MW_{th} CLG pilot plant.

agglomerate, leading to an increase in particle size and hence a decrease in the OC circulation rate within the system. These agglomerates need to be removed from the fluidized bed via sluicing to maintain the desired particle size distribution inside the reactor system.

- Deactivation: Thermal (e.g. sintering/melting) or chemical (e.g. ash interactions) impacts can lead to a decrease in the reactivity of the OC (i.e. lower oxygen carrier capacity or slower oxygen uptake/ release kinetics), impairing oxygen transport in the system and ultimately diminishing process efficiency.
- Ash Sluicing: In case feedstocks with high ash-contents are utilized, residual ash needs to be actively removed from the system via ashsluicing, leading to a gradual loss of OC material.

Due to the long-term operation at industry-like conditions, pilot tests inside the 1 MWth CLG unit used in this study present ideal conditions to investigate if the mechanisms listed above occur during CLG operation and if so, which one is the most dominant. In order to do so, samples from different positions in the 1 MWth pilot plant were collected during operation and subsequently analyzed with regard to their morphology, as well as physical (e.g. particle size and particle density) and chemical (e.g. oxygen transport capacity, redox rates) properties. Moreover, livedata from the process (e.g. OC make-up rates, mass extracted via filters and ash sluicing screws) was utilized to derive insights into the fate of the OC inside the 1 MWth CLG unit. Through combination of these unique datasets, this study closes a crucial research gap, thereby further promoting the technology readiness level of chemical looping processes towards market maturity.

2. Experimental

2.1. 1 MWth pilot plant

2.1.1. Pilot plant layout

The layout of the 1 MW_{th} CLG pilot plant is described in detail elsewhere [22]. Therefore, only the main features of the pilot, schematically shown in Fig. 2, are elaborated hereinafter for brevity.

The reactor system, consisting of an air reactor (0.59 m inner diameter, 8.66 m height), a fuel reactor (0.4 m inner diameter, 11.35 m height), and three coupling elements (two loop seals and a J-valve), is refractory lined to minimize heat losses, allowing for autothermal operation (i.e. without electrical heating. The AR can be fluidized with air or a mixture of air and recycled flue gas, which can be electrically pre-heated to temperatures up to 375°C. For process control reasons, the inlet gas composition (O2, CO2) is measured for the AR. The fuel reactor can be fluidized with air, steam, a mixture of steam and CO2, or a mixture of air and CO₂. The FR-fluidization media can be electrically pre-heated to temperatures up to 450°C. Each reactor is equipped with a cyclone for gas solid separation and a loop seal to prevent bypassing of gases. Global solid circulation between the two reactors is achieved with a J-valve, connecting the loop seal (LS) of the AR (LS1) with the fuel reactor. Each loop seal is equipped with a solid sampling facility, allowing for the controlled removal of OC samples during operation. More details on the sampling procedure are provided by Marx et al. [32]. The circulating mass flow between both reactors can be adjusted by changing the fluidization flow of the J-Valve, which can be fluidized with nitrogen or CO₂. For the fuel reactor, all entrained material leaving the riser is directly transferred into the AR via LS5, which is fluidized with nitrogen or CO2. On the other hand, the option of internal solid circulation via LS1, fluidized with nitrogen, exists for the AR. A solid fuel flow up to 340 kg/h corresponding to a thermal power of about 1.7 MW can be introduced into the dense bed of the FR via an oil-cooled feeding screw. The fuel reactor off-gases first pass a syngas cooler, where it is cooled to a temperature of approx. 350°C. Subsequently, the gas composition (CO, CO₂, O₂, H₂, CH₄) and gas flow is measured online. To allow for safe venting to the environment, the FR product gas is then

transferred through a hot gas filter, operated at up to 250°C, using an induced draft fan, before it enters a thermal oxidizer, required for full conversion of all hydrocarbon species to CO₂ and H₂O. The FR product gas can also be rerouted to a gas cleaning facility, equipped with a fuel synthesis test rig, if desired. After online gas sampling (CO, CO₂, O₂, SO₂, NO), the off-gases from the AR are cooled in a heat exchanger, to a temperature <250°C. Thereafter, the gas enters a fabric filter for dedusting. Downstream of the induced draft fan controlling the free-board pressure of the AR, the AR flue gases can be vented to the environment through a stack or can be partly recycled back to the AR airbox via the primary-air fan. In order to maintain constant reactor inventories throughout operation, the pilot is equipped with a make-up feeding system, allowing for the controlled introduction of up to 200 kg/h of ilmenite into the standpipe of LS1 via a dosing screw.

2.2. Materials

2.2.1. Bed material (1 MWth Pilot Plant) - ilmenite

Ilmenite from the Norwegian Company Titania AS, which was successfully deployed during previous chemical looping experiments in the 1 MW_{th} pilot [19,20,33], was used for the CLG experiments presented in this study. For the fresh material (ILMf), a bulk density of 2550 kg/m³, a particle density of 4486 kg/m³, and a mean particle diameter of 111 µm ($d_{p,10}=31~\mu\text{m}, d_{p,90}=224~\mu\text{m}$) was determined (more details see Section 2.4). For selected operating periods, a different granulation of ilmenite from the Norwegian Company Titania AS, was used. This coarser material (ILMc), exhibits a bulk density of 2336 kg/m³, a particle density of 4621 kg/m³, and a mean particle diameter of 199 µm ($d_{p,10}=151~\mu\text{m}, d_{p,90}=247~\mu\text{m}$) in fresh delivery condition.

2.2.2. Feedstocks

For CLG pilot testing in the 1 MW $_{th}$ facility, three different feedstocks were used. During the first test campaign (K1), cylindrical industrial wood pellets (IWP) conforming to the Norm ENPlus A1, purchased from Eckard GmbH, Germany, were used. For the second test campaign (K2), cylindrical pine forest residue pellets (PFR) from AB Torkapparater, Sweden were deployed. Throughout the third test campaign (K3), cylindrical pre-treated wheat straw pellets (WSP), from AB Torkapparater, Sweden, were utilized. Proximate and ultimate analysis as well as all pellet dimensions, bulk densities, and lower heating values (LHV) for all pellet types are given in Table 1.

2.3. Operating conditions of 1 MWth chemical looping gasifier

In 2022, the modular 1 MW $_{th}$ pilot plant at TU Darmstadt was continuously operated (24 h/day) as an autothermal chemical looping gasifier for approx. 14 days each in three separate test campaigns, yielding >400 h of chemical looping operation. These intervals of long-term operation allow for in-depth investigations of the fate of the OC during CLG.

Within the first test campaign (K1), the pilot was operated for $\sim\!110$ h in chemical looping mode, using industrial wood pellets as the feed-stock and fine ilmenite (ILMf) as the bed material. During the second test campaign (K2), the 1 MW_{th} pilot plant was operated using pine forest residue pellets as the feedstock, resulting in more than 210 h of successful chemical looping operation. Throughout the first section of K2, coarse ilmenite (ILMc) was used as the make-up bed material, before it was replaced with fine ilmenite (ILMf) in the later stages of the second test campaign. For initial reactor filling at the start of K2, old bed material from K1 was used. During the third test campaign (K3), the 1 MW_{th} pilot plant was operated using pre-treated wheat straw pellets as the feedstock and fine ilmenite (ILMf) as the bed material. 1 Here, the pilot

 $^{^{\}rm 1}$ Coarse ilmenite (ILMc) was utilized during system-start up, but was replaced with fine ilmenite (ILMf), before initiation of CLG operation.

plant was successfully operated in chemical looping mode for a total of ~ 80 hours.

2.4. Material characterization

During operation of the 1 MW_{th} pilot plant, solid material collected from both loop seals, both filters, and from the ash sluicing screw of both reactors were collected (sampling location see Fig. 2). These materials were analyzed using different lab techniques, in order to allow for the subsequent calculation of important evaluation parameters (see Section 2.5). Using the same methods, the fresh materials (see Section 2.2) as well as agglomerates, retrieved from the reactor after termination of K3 (more details see Section 3.4), were analyzed.

2.4.1. Particle size distribution (PSD) and mean particle diameter

The particle size distribution of the fresh materials and solid loop seal samples was determined according to the norm DIN66165, using an air jet sieve type LS200-N by the company Hosokawa Alpine AG, Germany. Each PSD was determined singularly. Based on the measured PSD, integral parameters, such as the mean particle diameter, were calculated for each bulk material.

2.4.2. Bulk density

Bulk densities for fresh materials and solid samples were determined using a self-made setup, consisting of a pouring device and a collection vessel with known volume, which conforms to the norm ISO 697. Values were determined in triplicates.

2.4.3. Particle density

Particle densities for fresh materials and solid samples were determined using according to the norm DIN EN ISO 1183, using water pycnometry in calibrated 25 and 50 mL pycnometers by Carl Roth, Germany. Prior to the measurements, the pycnometers were recalibrated using water at ambient conditions. During pycnometry, water temperatures were measured to account for the impact of changing room temperatures on water densities. All values were determined in duplicates. In case of strong deviations (>15 %) for two corresponding values, a third value was determined.

2.4.4. Attrition jet cup

Attrition behavior of the OC materials was evaluated using a jet cup according to the setup of Ryden et al. [34]. Inside the jet cup, the material was fluidized with air (600 NL/h), achieving nozzle velocities of approx. 100 m/s. For evaluation, each material was tested for 90 minutes, and the attrition was quantified at 10, 20, 30, 50, 70, and 90 minutes by weighing the filter located at the gas outlet of the jet cup.

2.4.5. Thermogravimetric analysis

Redox behavior as well as the oxygen transport capacity of the OC materials was evaluated via thermogravimetric analysis (TGA). Here, approx. 50 mg of OC material was heated to 950°C under $\rm N_2$ atmosphere. Subsequently, the OC material was firstly fully oxidized with synthetic air, at a flow rate of 100 mL/min for 20 min. Thereafter, the material was subjected to five redox cycles, using mild reduction and oxidation

conditions (reduction: 20 min, 100 mL/min of 6.5 vol.-% H_z , 35.5 vol.-% H_z O in N_z , oxidation: 20 min, 100 mL/min of synthetic air), to prevent substantial changes in the OC morphology occurring inside the TGA. Finally, the material was cooled down to ambient temperature under N_z atmosphere.

2.4.6. Pressure fluctuation tests

Using the fresh ilmenite OC (ILMf and ILMc, see Section 2.2.1), as well as ashes of the WSP (see Section 2.2.2), produced by muffle combustion at 700° C for 3 h, pressure fluctuation test were carried out following the method by Di Giuliano et al. [35–37], to evaluate the effect of WSP ashes on fluidization behavior of the utilized OC materials.

Here, ashes from biomass and OC were mixed at constant volumetric ratio (9 ml ash : 90 ml OC), and heated in a fluidized bed quartz reactor up to temperatures in the range $700{\text -}1000^\circ\text{C}$ with N_2 as the fluidizing agent. Pressure fluctuation signals were acquired at two and three times the minimum bubbling velocity of the OC at selected temperatures. Subsequent to the pressure fluctuation tests, samples from the fluidized bed were stored for SEM-EDS analyses (see Section 2.4.8).

2.4.7. Feedstock ash melting behavior

Ash of the different feedstocks was produced under gasification-like conditions in N₂/15 % H₂O/5 % CO₂ at 550°C. At the beginning, about 5 % O₂ was added to accelerate the carbon conversion until its concentration downstream of the sample, detected by a lambda sensor, increased to $\sim\!0.1$ %.

The melting behavior of the obtained ash was characterized by hot stage microscopy as described in literature [38,39]. Furthermore, the temperature-dependent melt fraction of the ash under equilibrium conditions was calculated using *FactSage* 8.1 and the *FactPS* (gas) and *FTOxid* (pure solids and SLAGA) databases. All major ash components Al₂O₃, CaO, Fe₂O₃, K₂O, MgO, Na₂O, P₂O₅ and SiO₂, recalculated from, were considered.

2.4.8. SEM, SEM-EDX, and SEM EDXRF analysis

Loop seal samples collected during operation of each test campaign, were analyzed via scanning electron microscopy (SEM) and SEM-energy dispersive X-ray spectroscopy (EDX), to determine the distribution of Fe, Ti, Ca, Si, and O on the particle surface. Moreover, micrographs were taken from selected samples and these micrographs were analyzed via SEM-EDX, to map the given elements along the particle diameter.

Additionally, pieces of the agglomerated samples from K3 (more details see Section A.3 in the Supplementary Material) were ground in a mortar and the resulting powder was characterized by EDX- fluorescence spectroscopy (EDXRF) and X-Ray Diffraction (XRD) regarding elemental and mineral composition, respectively. Unground material of the same samples were investigated by SEM-EDX.

Lastly, SEM-EDX analysis of the resulting materials from the pressure fluctuation tests (see Section 2.4.6) was carried out, to visually assess potential changes in particle structure.

Table 1
Proximate (as received), ultimate analysis (dry ash free) and other properties for industrial wood pellets (IWP), pine forest residue pellets (PFR), and wheat straw pellets (WSP).

	IWP Ultimate in	PFR wt% (d.a.f.)	WSP		IWP Proximate in	PFR wt% (a.r.)	WSP		IWP Other Prope	PFR erties	WSP
С	50.8	48.9	42.5	C-fix	13.3	16.63	16.3	d [mm]	6	6 - 8	6 - 8
Н	6.0	5.8	5.10	Volatiles	79.6	76.77	68.7	1 [mm]	10 -25	8 - 12	8 - 12
O	43.2	38.3	36.7	Ash	0.65	2.20	4.2				
N	0.07	0.43	0.10	Moisture	6.5	4.40	10.8	ρ _{bulk} [kg/m ³]	650	630	504
S	0.008	0.02	0.48					LHV [MJ/kg]	17.96	18.3	15.3
C1	0.006	0.01	0.07					_			

2.5. Evaluation parameters

2.5.1. OC oxygen carrying capacity

The oxygen carrying capacity of the OC is calculated by relating the oxidized (m_{Ox}) and reduced (m_{Red}) masses of the OC [24]. These masses are determined at the end of the oxidation and reduction step inside the TGA (see Section 2.4.5), respectively:

$$R_{OC} = \frac{m_{Ox} - m_{Red}}{m_{Ox}} \tag{1}$$

2.5.2. OC redox rate index

To determine the redox reaction rates of different OC samples, the relative weight (ω) of the OC inside the TGA is defined as:

$$\omega(t) = \frac{m(t)}{m_{Ox}} \tag{2}$$

Using this value, the rate index, suggested in literature [23], can be calculated by:

$$RI \left[wt. - \%/min \right] = 60 \cdot 100 \cdot \left(\frac{d\omega}{dt} \right)_{norm} \tag{3}$$

Here, the last term signifies the normalized relative weight change of the OC ($d\omega$) over time and is calculated by adjusting the weight change determined inside the TGA ($_{exp}$) with reference partial pressures for the reducing or oxidizing gases [27]:

$$\left(\frac{d\omega}{dt}\right)_{norm} = \left(\frac{d\omega}{dt}\right)_{exp} \frac{p_{ref}}{p_{TGA}} \tag{4}$$

For the oxidation, a reference oxygen partial pressure of 0.1 atm was used, whereas for the reduction a reference hydrogen partial pressure of 0.15 atm was employed [27]. The experimental weight change rate of the OC is calculated via linear regression of the weight vs. time data from the TGA over the first 40 s of reduction and 16 s of oxidation, respectively. In this duration, a relative weight change $(\Delta\omega)$ of approx. 0.01 is obtained, for which it was found that OCs generally exhibit fast and constant oxygen release and uptake kinetics [23].

2.5.3. OC lifetime

Another important parameter for scale-up of the chemical looping technologies is the OC lifetime. In smaller continuous chemical looping pilots, this parameter relates the fines losses (<40– $45 \mu m$) to the total OC reactor inventory ($m_{inv.}$) [29,40]. For the 1 MW_{th} CLG system, a similar definition is used. However, in addition to fine losses towards the filters (Δm_{FA}), the material removed from the AR and FR via ash sluicing (Δm_{BP}) over a given period of time (Δt) is also considered here:

$$\tau_{LT,OC} = \frac{m_{inv.} \cdot \Delta t}{\Delta m_{FA,AR} + \Delta m_{FA,FR} + \Delta m_{BP,AR} + \Delta m_{BP,FR}} \approx \frac{m_{inv.}}{\dot{m}_{MU,OC}}$$
 (5)

A method to approximate the OC lifetime ($\tau_{LT,OC}$) for the 1 MWth CLG plant is by relating the reactor inventory to the OC make-up rate ($m_{MU,OC}$), necessary to stabilize the AR and FR reactor inventory.

2.5.4. OC attrition index

One factor determining the OC lifetime is its stability towards attrition. Using the jet cup (see Section 2.4.4), the attrition behavior of the OC in a lab environment was analyzed. For further analysis, an attrition index (*AJI*) similar to the one defined by Ryden et al. [34] was defined:

AJI
$$[wt. - \%/h] = 100 \cdot \frac{m_{fines}(t = 90 \text{ min}) - m_{fines}(t = 30 \text{ min})}{m_{0,OC}}$$
 (6)

Here, $m_{0,OC}$ denotes the mass of the OC placed into the jet cup prior to experiment, and $m_{\rm fines}$ is the mass of fines collected from the filter at the outlet of the jet cup at 90 and 30 minutes.

2.5.5. Cyclone efficiency

The cyclone efficiency (η_{Cyc}) is another important parameter affecting the OC lifetime, as it decides to which extent OC particles can be maintained inside the system. The cyclone efficiency is defined as follows:

$$\eta_{Cyc} = 1 - \frac{\Delta m_{FA}}{\dot{m}_{circ.OC} \cdot \Delta t} \tag{7}$$

Here, Δm_{EA} denotes the fine losses over a given period of time (Δt), while $m_{circ.,OC}$ is the global OC circulation rate, determined via the method of Marx et al. [32].²

3. Results and discussion

The effect of CLG operation on the OC inside the 1 MW_{th} pilot plant will subsequently be analyzed in four dedicated sections. Firstly, characteristic changes in OC morphology and composition arising during chemical looping operation will be discussed in Section 3.1. Subsequently, changes in the physical properties of the OC (e.g. particle size, particle density, etc.) will be analyzed in Section 3.2. Thereafter, changes occurring in the OC's chemical properties during redox cycling in the 1 MW_{th} CLG system will be highlighted in Section 3.3. Lastly, the effect of feedstock characteristics on OC properties, observed during operation with wheat straw pellets, will be presented in Section 3.4. In doing so, a holistic overview over the fate of the OC in industry-like CLG conditions will be provided.

3.1. Morphological and compositional changes of OC

It is well established that OC particles undergo distinct morphological and compositional changes during chemical looping operation. For one, the particle porosity increases as macro-pores in the range of 50-500 nm are formed within the OC particle [26]. This distinct change in OC morphology was also observed during 1 MWth CLG operation, which is not only deducible from the change in particle density (see Section 3.2.2), but is also clearly visible in SEM micrographs of fresh and used OC particles. As visible in Fig. 3, showing micrographs of fresh (Fig. 3a and b) and used (Fig. 3c and d) OC samples, pores form on the inside of the OC during CLG operation, induced through the oxygen migration during the redox activity of the OC inside the FR and AR. This arise of macro-pores inside the OC particle was found to be crucial for OC activation and reactivity [27], making it an important phenomenon in chemical looping operation. The observation of this phenomenon inside the 1 MWth CLG unit shows that it occurs regardless of reactor size and operational mode, meaning that it will also occur in an industrial-size CLC/CLG unit. As more porous OC particles generally exhibit weaker mechanical properties [23], it can be inferred that the observed pore formation is one reason why used OC particles from the 1 MWth CLG unit exhibit a lower mechanical stability than the fresh OC (see Section A.2 in the Supplementary Material). Moreover, the increased porosity leads to faster oxygen release and uptake by the OC [27], improving the overall redox kinetics (more details see Section 3.3).

Another phenomenon giving rise to the increase in OC particle porosity during chemical looping operation is the well-documented formation of a detached iron-rich layer at the surface of the OC [26–29]. This shell-formation does not only entail the formation of a porous layer between the shell and the core [26,27], which increases particle porosity, but the underlying iron migration was found to lead to cracks inside the OC particle [26,27], also entailing a decrease in particle density. To determine to which extent this behavior occurred

 $^{^2}$ Since the solid entrainment from the AR exceeds the global OC circulation for the given setup of the 1 MW_{th} CLG unit, cyclone efficiencies determined for the AR signify minimum values.

during 1 MW_{th} CLG operation, selected OC samples were analyzed via SEM-EDX. Micrographs analyzed via SEM-EDX clearly show the formation of a Fe-rich and Ti-depleted shell during CLG operation (see Fig. 4a and c). Further SEM analysis showed the fracturing-off of pieces of the iron-rich shell (see Fig. 4b and c), indicating that the boundary between bulk and shell constitutes a weak point of the OC particle. This means that, as mechanical forces act upon the OC particle inside the CLG system, the shell-layer is easily broken-off and hence is a major reason for particle abrasion. As the growth of the iron-enriched shell was found to increase with increasing redox activity of the particle [26] this finding could explain why lower OC lifetime are reported for CLG when compared to CLC [29], as the OC reaches deeper reduction stages for the former, thus favoring shell-growth and subsequent shell-abrasion.

3.2. Change of physical properties of OC during 1 MW_{th} pilot testing

It is generally known that physical properties of the OC are of high importance for the operation of chemical looping systems. For example, the OC has to exhibit particle sizes in the right range to achieve sufficient solid circulation and prevent extensive material loss [41]. Moreover, a certain material rigidity is required, to prevent extensive material losses via abrasion and/or fragmentation [24]. Here, ilmenite was found to be a promising material, exhibiting lifetimes >500 h due to its good mechanical stability [25,26]. Moreover, ilmenite was successfully used for chemical looping combustion in 1 MWth scale [19,33], underlining its availability in the required particle sizes. Thus, ilmenite is generally considered to be a material well-suited for chemical looping operation [24,25]. Nonetheless, detailed analyses of the physical changes occurring in ilmenite particles in an industry-like chemical looping setup have not been reported in literature, yet.

3.2.1. Particle size distribution, attrition behavior and OC lifetime

A straightforward method to determine the fate of the OC inside the CLG system and evaluate changes of its physical properties during operation is to close the solid mass balance around the CLG system. In literature, OC lifetimes of 1300 and 630 h were reported for ilmenite for continuous CLC and CLG operation in the 1.5 kWth range, respectively, by recovering and weighing the fines (<40 µm) collected in the filters during operation [29]. For the 1 MW_{th} pilot plant, a similar procedure can be employed, i.e. by continuously weighing the collecting containers from both filters as well as the material removed via ash sluicing during operation (see Eq. (5)). In contrast to smaller units, the OC make-up system is used to stabilize the solids inventory of the 1 MWth CLG system during operation (approx. 1200 kg), thus signifying a source of fresh material input into the system. The second solid material fed into the reactor system is the feedstock, which is being introduced inside the FR. Here, feedstock moisture and volatiles leave the FR in a gaseous form. Moreover, the fixed carbon can be assumed to be almost entirely converted into gaseous species inside the reactor system (FR & AR), meaning that only feedstock ash remains in its solid state inside the CLG unit. Consequently, the solid input accumulating in the CLG system constitutes the sum of the fed fresh OC and the ash from the feedstock fed into the FR.

When calculating the total solid input for a five-day period of stable chemical looping operation from K1, a value of approx. 3.6 t is obtained. As shown in Fig. 5, the vast majority of those 3.6 t can be attributed to fresh OC material, since the wood pellets used as feedstock contain only minor amounts of ash (see Table 1). As a basic rule, the bed material can leave the reactor through two pathways: (i) in the form of fines travelling through the cyclones towards the AR or FR filter together with the gas stream, and (ii) from the bottom of the reactor beds through the ash sluicing screws. While the extent of the former pathway is plant- and material-specific and can hardly be impacted by the operating

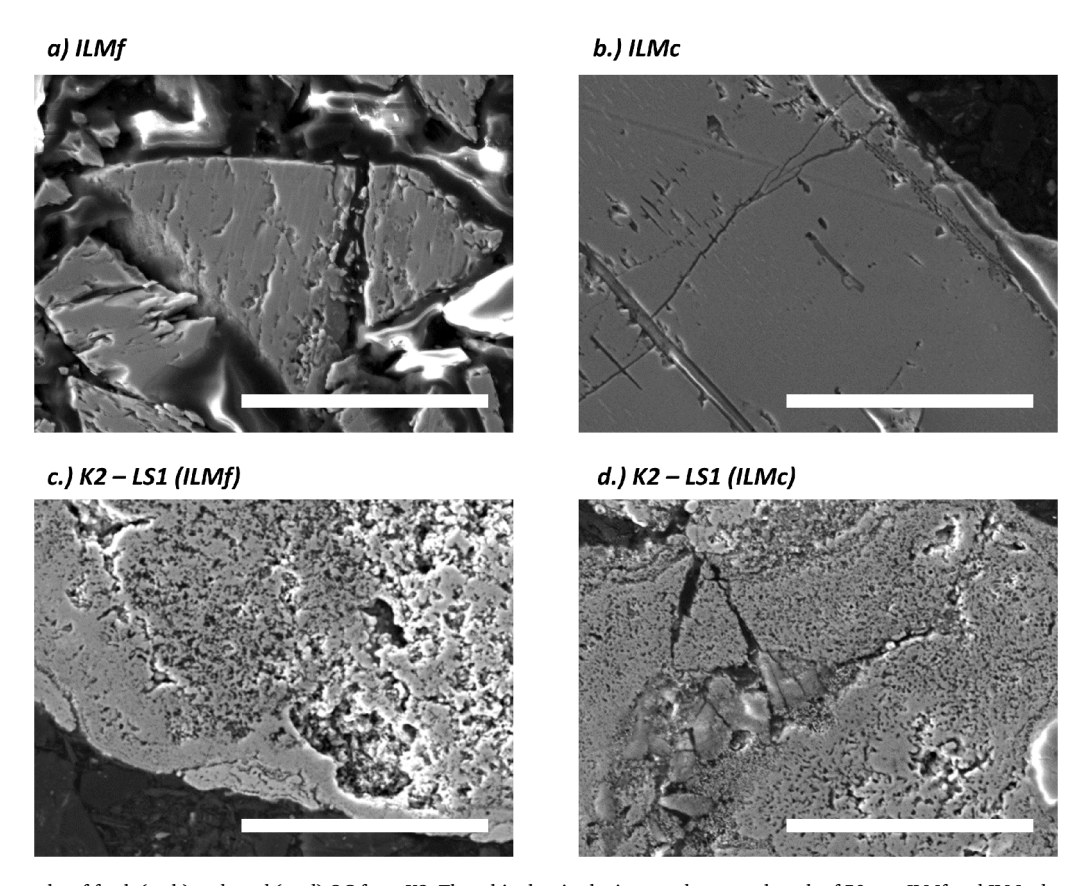


Fig. 3. SEM micrographs of fresh (a+b) and used (c+d) OC from K2. The white bar in the images denotes a length of 50 μ m. ILMf and ILMc denote the two different ilmenite granulations (see Section 2.2.1).

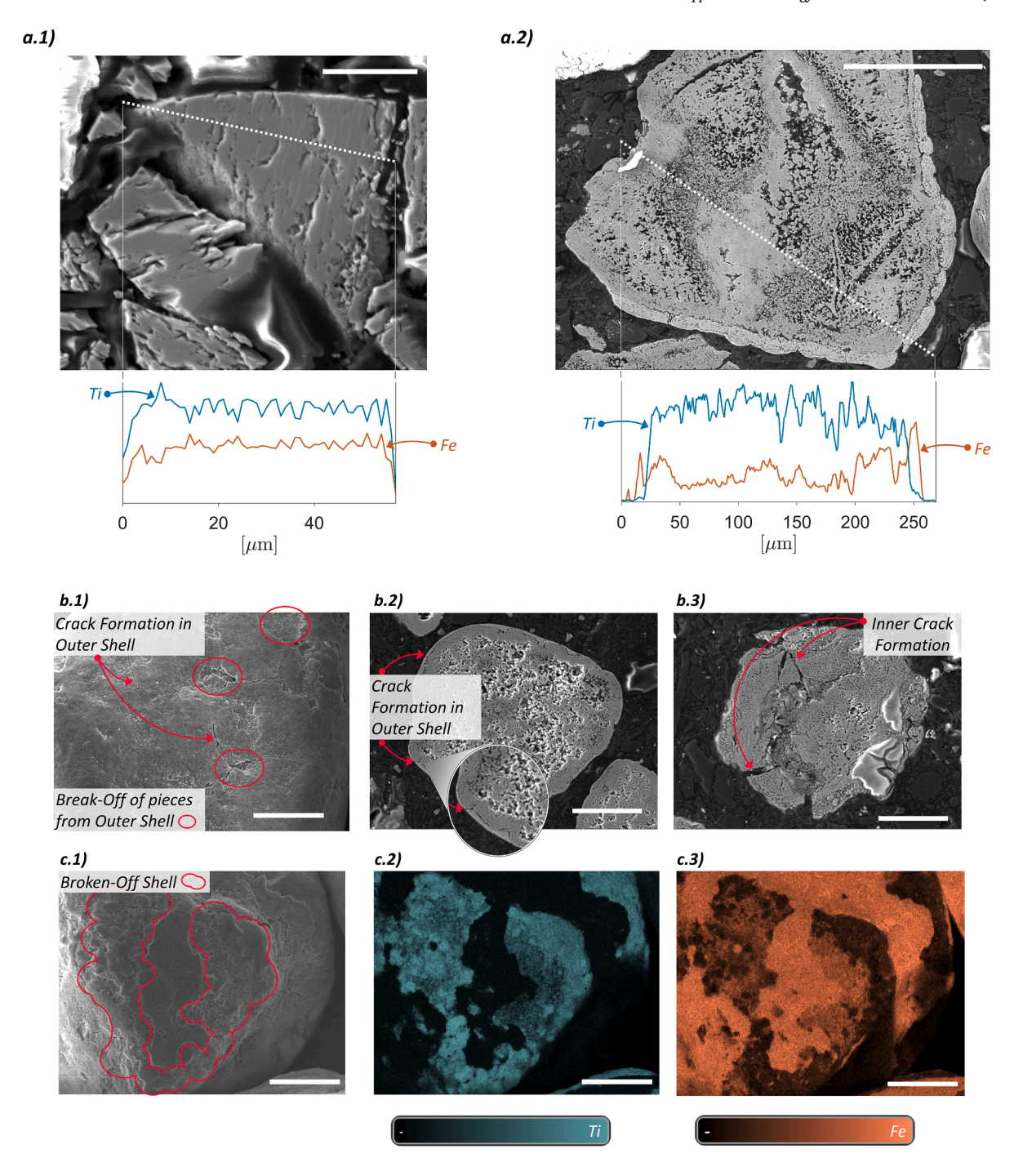
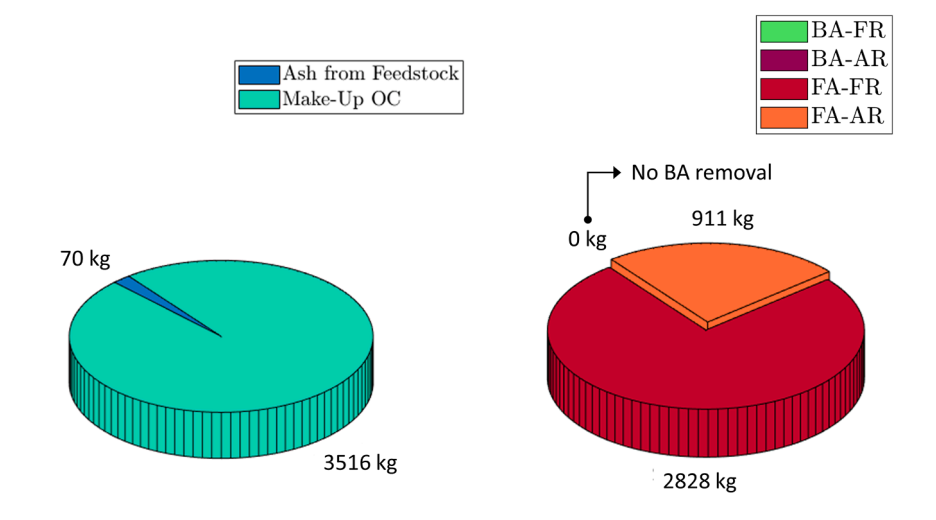


Fig. 4. SEM/SEM-EDX images and micrographs of OC samples. a.1) SEM micrograph of fresh ILMf with line scan indicating concentration of Fe and Ti (white bar: 20 μm). a.2) SEM micrograph of utilized OC from K2 with line scan indicating concentration of Fe and Ti (white bar: 50 μm). b.1) SEM image of utilized OC from K2 with indications of cracks and broken-off shell (white bar: 50 μm). b.2) SEM micrograph of utilized OC from K2 showing cracks in the outer Fe-rich layer (white bar: 50 μm). b.3) SEM micrograph of utilized OC from K2 showing long cracks reaching into the particle bulk (white bar: 50 μm). c.1–3) SEM-EDX image of utilized OC from K2, with indications of zones where the Fe-rich layer broke off during operation (1), and the respective Ti (2) and Fe (3) content (white bar: 50 μm).

conditions, ash sluicing is a dedicated procedure that only becomes necessary in case changes in the bed material, such as ash accumulation, agglomeration, or deactivation occur to relevant extents. As shown in Fig. 5, this was not the case during pilot testing in the 1 MW $_{th}$ scale with industrial wood pellets, as material was not extracted from the reactor system during 125 h of steady state operation. In contrast to that, approx. 3.7 t of material was retrieved from the AR and FR filter, with over 75 % of the material ending up in the FR filter. Similar findings were also made for stable chemical looping operation with the fine

ilmenite (ILMf) during K2, showing that the trends observed for K1 are reproducible (more details see Section A.1 in the Supplementary Material).

To be able to answer why the material is lost in the AR and FR cyclones, a detailed analysis of the solid samples from the 1 MW $_{th}$ unit is necessary. One important variable for cyclone efficiencies is the particle size of the material, as depending on the size of the particle surface forces or inertial forces dominate inside the cyclone, leading either to their separation from the gas stream or to their losses towards the filter



Operational Duration: 124.7 h

Fig. 5. Solid mass balance around CLG unit for K1 between 9th April 2022 18:00 and 14th April 2022 22:40. Left: Solid material fed into the CLG unit, Right: Solid material extracted from the CLG unit.

[42]. Fig. 6 shows the cumulative particle size distributions (PSD) of the following samples taken during steady state CLG operation from the 1 $\rm MW_{th}$ unit:

- BA-FR: Particles from the bottom of the bed of FR,³
- BA-AR: Particles from the bottom of the bed of AR,³
- LS-FR: Particles from LS5,
- LS-AR: Particles from LS1,
- FA-FR: Particles from the FR Filter,
- FA-AR: Particles from the AR Filter.

It is visible that the material collected from the two filters (AR & FR) exhibits a significantly higher content of fines in comparison to the fresh OC material, whereas the opposite is true for the material extracted from the reactor beds via ash sluicing (i.e. it contains a higher content of coarse particles). The PSDs of the material extracted from both loop seals fall in between those extracted from the filters and from the ash sluicing screws, yet exhibit a lower fraction of fines in comparison to the fresh ilmenite. The resulting mean particle diameter of the material cycling through the CLG system amounts to approx. 130 µm, which is similar to the one previously obtained during CLC operation (=154 μm) in the 1 MW_{th} pilot [19]. These observations can be explained as follows. Ultimately, the fresh OC material fed into the system enters via the stand-pipe of LS1 (see Fig. 2) and is subsequently distributed inside the reactor system. Coarse particles, either from the fresh OC material or agglomerates formed during operation accumulate at the bottom of the reactors and/or the loop seals and are thus primarily found in the samples collected from the bottom beds of both reactors. On the other hand, fine particles which cannot be separated from the gas streams in the cyclones, stemming either from the fresh OC material, from fines formed during attrition of the OC, or from ash compounds from the solid feedstock fed into the FR, leave the reactor system towards the filters and are collected there. Intermediated-size particles in the range of $60-250 \mu m$ continuously cycle through the system and are thus found primarily inside the reactor system and hence are being sampled from both loop seals. Apart from these straightforward conclusions, the absence of fine particles <60 μm and the low fraction of particles in the range of 60–100 µm inside the loop seal samples (see Fig. 6), suggest that the fine particles are lost during operation. Interestingly, visibly more particles with diameters ${>}60~\mu m$ are found in the FR filter compared to the AR filter, suggesting that the FR cyclone exhibits a lower separation efficiency than the AR cyclone, which also explains why significantly more material was lost through the FR filter (see Fig. 5). When considering the PSDs for both fly ash samples in Fig. 6, it is clearly visible that substantial amounts of particles with diameters ${>}40~\mu m$ are retrieved in the filters (AR: 14 wt.-%, FR: 37 wt.-%), meaning that for the 1 MW_{th} pilot, significantly lower OC lifetimes than for other setups, where only fines with diameters smaller than 40–45 ${\mu}m$ are recovered [29,40], can be expected.

Due to the pronounced presence of fine particles inside the fresh OC, the fines collected in the filters stem directly from the fresh material fed into the CLG system to a significant extent. When considering the PSD of the fresh OC it can be stated that approx. 25 wt.-% of the fresh material (<60 µm, see Fig. 6) will be lost rapidly inside the CLG system via the cyclones. The remainder of the fines collected in both filters can be attributed to fine formation through attrition. When considering the entire fines collection of 3739 kg in both filters for the operating period under investigation (see Fig. 5), it can be conjectured that at least $23.5\,\%$ (879 kg) of that material directly stems from fine fraction of the fresh OC material fed into the system, which lies below the cut point of the FR cyclone (see grey shading in Fig. 7a). On the other hand, approx. 2141 kg can be directly attributed to attrition of coarser particles into fines, which is illustrated in Fig. 7b. Using this number, an attrition rate of 17.2 kg/h can be calculated for the 1 MW_{th} pilot plant for the duration under investigation, which translates into an OC lifetime of 69.8 h (see Eq. (5)).

The most obvious measure to increase OC lifetimes would be an optimization of the FR cyclone to allow for a more efficient removal of fines. When taking into account the average OC circulation rate of $14,974 \, \text{kg/h}$, determined using the method of Marx et al. [32], an average separation efficiency (see Eq. (7)) of $99.84 \, \%$ and $99.95 \, \%$ can

 $^{^{\}rm 3}$ Material was extracted via ash sluicing at the end of the experiment (i.e. during system shut-down).

⁴ Feedstock ash and unconverted char escaping via the AR & FR cyclone are not considered here. Through considerations of these solid species, slightly higher OC lifetimes would be obtained, albeit the impact is expected to be minor.

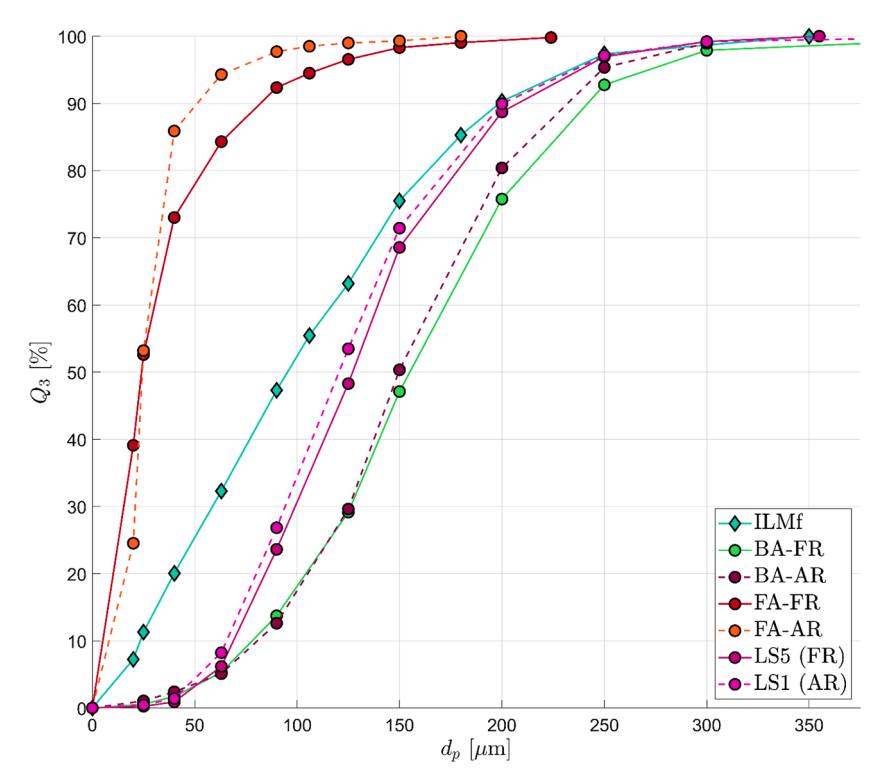


Fig. 6. Cumulative particle size distribution (PSD) of ilmenite samples collected from different positions during operation of the 1 MW_{th} pilot. All samples were collected between 14th April 2:30 am and 15th April 11:00 am during CLG operation.

be calculated for the FR and AR cyclone for the operating period under investigation, respectively, leaving room for improvement. As a reference, cyclone efficiencies up to 99.99 % were found to be obtainable by tailoring cyclone inlet geometries for a 8 MWth dual fluidized bed gasification (DFBG) system [44], meaning that material losses esp. towards the FR filter could be substantially reduced. For example, material losses via the cyclones would decrease by 26.5 %, in case the cut points for both cyclones were shifted to 40 μm , meaning that OC lifetimes up to 95.0 h would be achieved. Another potential measure to reduce material consumption in the 1 MWth unit would be to tailor the PSD of the fresh OC (e.g. via sieving), to prevent direct material losses of the fines contained in the fresh material. In an attempt to reduce material consumption, old bed material from K1 and coarse Ilmente (ILMc) was used during K2. Here, it was found that material losses were drastically reduced, yielding OC lifetimes of up to 170 h. 6 On the one hand, this was related to the fact that fine losses from the fresh material were completely eliminated. Moreover, as the average particle diameter of the coarse ilmenite (=199 µm) lies further away from the cut-point of the FR cyclone, attrition of the larger OC particles does not lead to a direct loss of those via the cyclone (more details see Section A.1 in the Supplementary Material).

However, even when tailoring the fresh OC PSD and optimizing cyclone geometries, substantially lower OC lifetimes (<500 h) than reported for smaller units in literature are expected to be obtained in the 1 MW_{th} unit. A comparison of SEM images of OC samples from both loop seals, shown in Fig. 8, suggests that attrition follows a similar mechanism as observed in smaller units. Here, it was found that particle rounding and detachment of outer particle layers drive attrition rates, as

opposed to particle fragmentation [26,28], which is also suggested by the recorded SEM images (more details see Section 3.3). The obvious similarity in the governing mechanism leaves the question why attrition rates observed in the 1 MW $_{\rm th}$ unit exceed those previously reported in literature

On the one hand, this could be related to greater mechanical stresses in the 1 MWth pilot plant, leading to a more severe mechanical strain on the OC particles. In terms of acting mechanical forces, reactor geometry and configuration play an important role in chemical looping systems [45]. For fluidized bed configurations it is known that jet and cyclonic attrition effects dominate particle attrition, with both factors increasing in effect with increasing gas velocity [28]. As gas velocities (u_0) up to 7 m/s in the FR are necessary to achieve the required solid circulation in the 1 MW_{th} unit [46], it becomes obvious that larger mechanical stresses act on the OC inside the given CLG system, when compared to smaller pilots where generally lower gas velocities are employed (impact forces scale with u_0^2 , frictional Stoke forces with u_0). Additionally, the inner refractory lining of the riser, cyclone, loop seals and stand-pipe of the 1 MWth unit exhibits a rougher and more uneven surface than their steel counterparts used in smaller setups [29,47,48]. On the one side, this leads to increased wall-particle friction, while it also decreases smoothness in the particle trajectory, thus making particle-particle impacts more likely. Consequently, it can be stated that due to the combination of those boundary conditions, the mechanical strain on the OC particles is larger for the 1 MW_{th} unit in comparison to smaller pilots, for which OC lifetimes >500 h were determined [29].

Another factor playing into the OC lifetime are the chemical stresses acting on the OC during redox cycling. It is generally accepted, that the particle's attrition resistance decreases through the intrinsic morphological changes induced through redox cycling [26,28,45,49-51] (see also Section 3.1). This was also shown for the 1 MW $_{th}$ CLG unit, with samples exposed to longer redox cycling durations showing higher attrition rates in the jet cup (see Section A.2 in the Supplementary Material). With deeper OC reduction stages being obtained for CLG when compared to CLC [52] it was found that OC lifetimes decrease for

⁵ The comparably high separation efficiencies can be attributed to the high solid loadings in the gas streams leaving the AR and FR, which are known to enhance cyclone separation efficiencies [43].

 $^{^6}$ However, utilization of ILMc led to sub-optimal CLG efficiency, mainly related to insufficient solid circulation rates between the AR and FR, making its utilization in the 1 MWth CLG system unbeneficial.

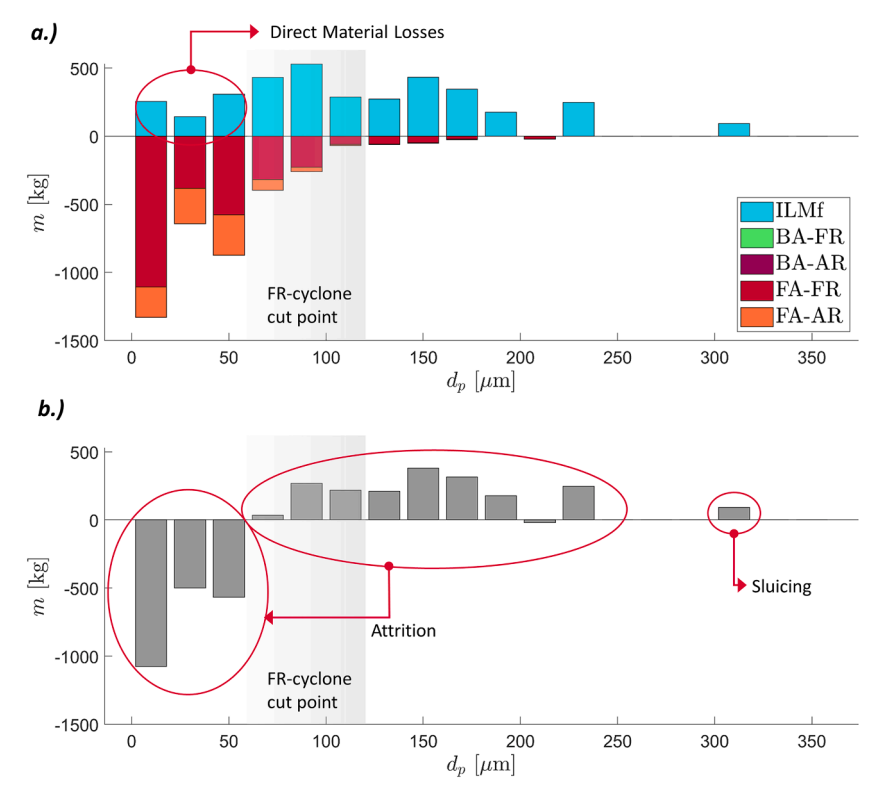


Fig. 7. a) Particle specific input (+) and output (-) of solids from 1 MW_{th} pilot between 9th April 2022 18:00 and 14th April 2022 22:40. b) Net particle specific solid in-/output between 9th April 2022 18:00 and 14th April 2022 22:40.

the former [29]. However, as the chemical stress in the 1 MW_{th} unit is not different to that in smaller setups, it has to be summarized that the comparably shorter OC lifetimes observed in the 1 MW_{th} CLG unit cannot be attributed to it.

Lastly, the thermal strain on the OC in the 1 MWth CLG unit could potentially lead to increased attrition rates. The amplifying effect of temperatures on OC attrition is reported in literature [28,50]. While all CLC/CLG systems are operated at elevated temperatures leading to a certain thermal strain on the OC particles, they are exposed to additional thermal stresses in an autothermal CLG setup such as the 1 MWth unit, due to the temperature difference between AR and FR. This temperature difference means that the OC particles are rapidly cooled down upon entering the FR and are heated up again upon entering the AR. With temperature differences in the range of 100 K being observed in autothermal systems [32,52], the repeated temperature increase/decrease could lead to substantial weakening of the OC structure. Another factor which needs to be considered is that because of this temperature difference between AR and FR, the OC is generally exposed to higher maximum temperatures in an autothermal setup. This factor becomes of an even greater relevance, when considering the results by Nelson et al. [28], who found that ilmenite attrition rates increase sharply between 895 and 970°C from 0.9 wt.-%/h to 3.2 wt.-%/h in a modified air-jet setup.8 This finding suggests that there exists a critical temperature threshold above which OC attrition increases sharply and due to the intrinsic properties of the CLC/CLG process, the exceeding of this threshold is more likely in an autothermal setup.

In summary, it can thus be stated that the relatively low OC lifetimes observed for the 1 MW_{th} CLG pilot plant result from an interplay

comparably low (FR) cyclone efficiency and the PSD of the fresh OC material, increased mechanical stresses induced through harsher process conditions (e.g. u_0) and reactor materials, and increased thermal stresses due to inherent peculiarities of the autothermal CLG process.

3.2.2. Bulk and particle density

Apart from particle size and attrition rate, particle density is a crucial property of any material used in fluidized beds [53]. Fig. 9 shows that in contrast to the average particle diameter, which rapidly reaches a constant unchanged value inside the CLG system (see Fig. 9a), particle as well bulk densities of the OC material cycling through the system change gradually with increasing operating time. Clearly, all values determined for LS samples during operation lie distinctly below the ones determined for the fresh material. Moreover, it is visible that particle densities decrease with increasing operating time, indicating an increasing particle porosity, induced through redox cycling [26] (more details see Section 3.1). Similarly, bulk densities also decrease with increasing operating time, with changing particle porosity and shape. Both decreasing trends are interrupted by a phase of increased make-up feeding on 11th April, where reactor inventories were increased by the plant operators (see Fig. 9d). Here the effect of the large quantities of freshly fed material on the both densities is clearly visible, shifting the average particle and bulk density towards the properties of the fresh OC (see red arrows in Fig. 9b and c). On the other hand, the average particle diameter is unaffected by the increased make-up rates, underlining the hypothesis that the fines from the make-up material are rapidly lost during operation (more details see Section 3.2.1). Subsequent to the feeding of the fresh material on April 11th, the decreasing trend in both densities continues, underlining the continued occurrence of morphological changes in the OC particles during CLG operation. These changes in particle morphology were also observed during chemical looping combustion operation and were found to go in hand with a decrease in particle rigidity [26]. Consequently, it can be summarized that for the given make-up rates and in the absence of bed material sluicing, densities of the OC particle decrease continuously, indicating ongoing

 $^{^7}$ E.g. for a FR temperature of 875 °C, the max. system temperature in an externally heated setup amounts to 875-900 °C, while it amounts to 975-1000 °C in an autothermal setup.

⁸ An attrition rate of 3.2 wt.-%/h would translate into an OC lifetime of approx. 31 h, falling into the same range as observed in the 1 MW_{th} CLG unit.

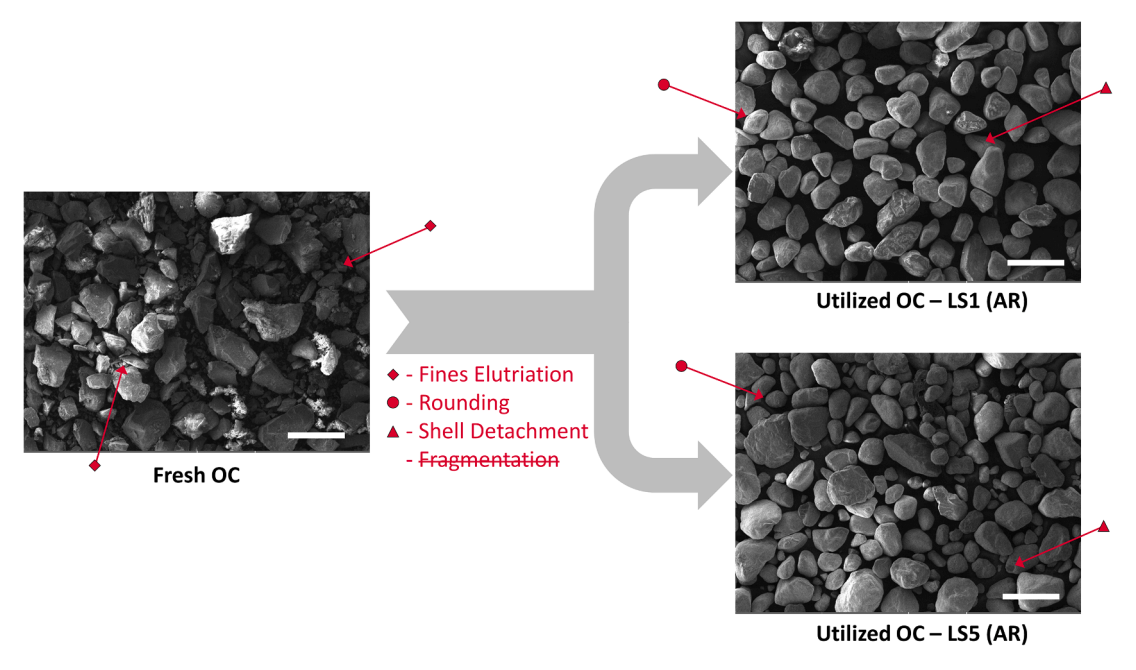


Fig. 8. SEM images of fresh (left) and utilized (right) OC material from K1. Arrows with diamonds at the end indicate fines in the fresh material no longer present in the utilized OC, arrows with circles indicate rounded OC particles and arrows with triangles indicate particles with a broken-off or cracked shell.

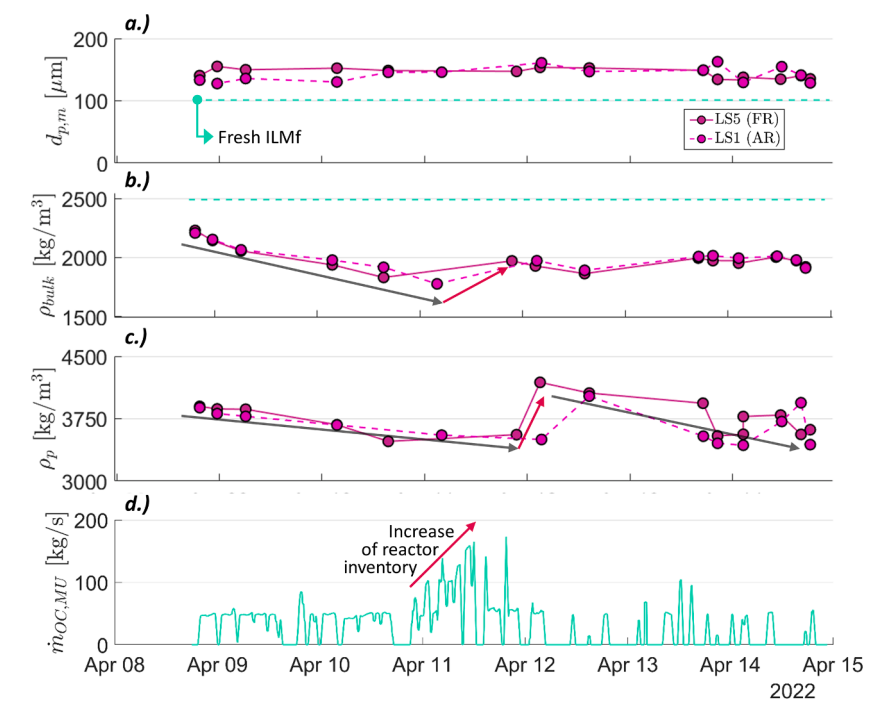


Fig. 9. Change of particle properties from LS1 and LS5 between 8th April 2022 18:00 and 14th April 2022 22:40 (K1). Dashed blue line indicates the properties of fresh ilmenite - a) Average particle diameter, b) bulk density, c) particle density. d) Make-up feed of ilmenite into 1 MW_{th} pilot between 8th April 2022 18:00 and 14th April 2022 22:40.

morphological changes inside the OC particles. For the given operating times, fully constant values for bulk and particle densities were not obtained in the 1 MW $_{th}$ unit. However, upon consideration of Fig. 9 it can be stated that a bulk density of $\sim\!1800~kg/m^3$ and a particle density of $\sim\!3400\!-\!3500~kg/m^3$ can be expected for the OC bed material during continuous CLG operation.

3.2.3. Summary

Based on the observations of the mechanical properties of the OC

particles during CLG operation, it can be summarized that mechanical and chemical strains lead to a decrease in particle diameter, particle density, and bulk density with elapsing operating time. When woody biomasses (IWP and PFR) were used as the feedstock, material deactivation or agglomeration do not determine the lifetime of the OC inside the 1 MW $_{\rm th}$ unit. Rather, material losses through the cyclones defined the necessary make-up rates, with OC lifetimes observed in the 1 MW $_{\rm th}$ pilot plant being significantly lower than those observed in smaller pilots.

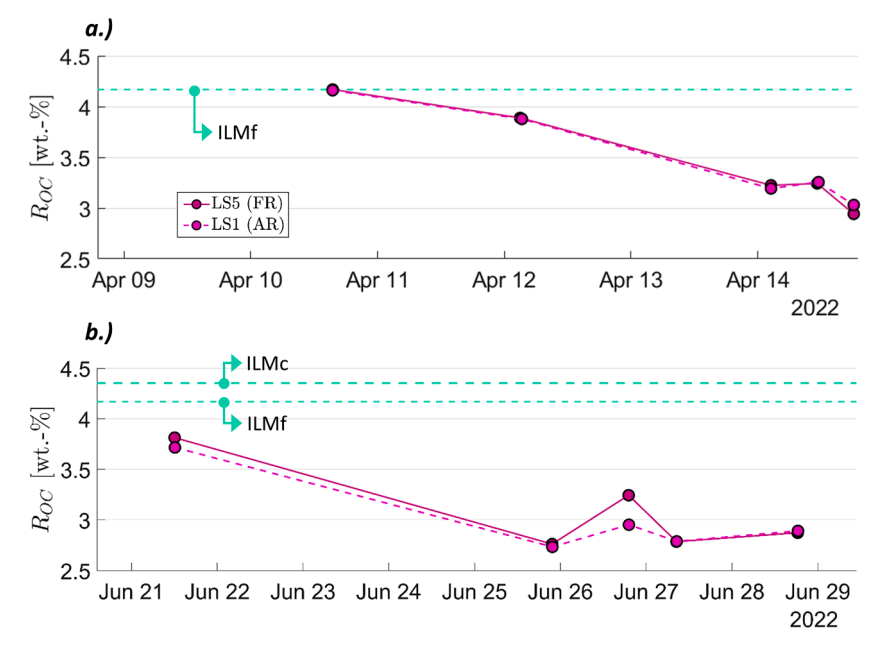


Fig. 10. a.) Change of oxygen carrying capacity of samples from LS1 and LS5 between 8th April 2022 19:00 and 14th April 2022 122:40 (K1). b.) Change of oxygen carrying capacity of samples from LS1 and LS5 between 20th June 2022 10:00 and 29th June 2022 12:00 (K2). Dashed blue line indicates the properties of fresh ilmenite (ILMc, ILMf).

On the one hand, the comparably low OC lifetimes can be attributed to peculiarities of the 1 MW_{th} pilot, such as the high gas velocities required in the FR in order to attain the necessary OC circulation rates or the low separation efficiency of the FR cyclone. On the other hand, reactor materials (refractory lining) and process conditions (e.g. ΔT between AR and FR), present in any industry-like or industry CLG setup such as 1 MW_{th} pilot plant, are expected to lead to decreased OC lifetimes, when compared to smaller pilots.

To optimize OC lifetimes in a full-scale setup, the following measures are therefore suggested:

- Optimization of cyclone geometries to minimize losses of particles >40 µm,
- Tailoring of PSD of fresh OC (e.g. removal of all fines with $d_p < 30$ –40 μ m) to minimize direct losses of fresh material,
- Equipment of the CLG system with a secondary solid removal unit operation downstream of the cyclone, to remove the coarser fraction of the fines and allow for its subsequent reintroduction into the CLG unit.⁹

All in all, it is believed that by implementing those approaches, OC lifetimes could be increased beyond 300 h for a full-scale CLG unit, meaning that procurement and waste removal costs should not pose a substantial barrier for implementation from a technical or economic perspective [56].

3.3. Change of chemical properties of OC during 1 MWth pilot testing

Apart from the physical changes the OC particle undergoes in a

chemical looping system, which were detailed in Section 3.2, the chemical strain induced on the OC during redox cycling also entails changes in the chemical properties of the OC. The impact of CLG operation on the OC oxygen transport capacity is elaborated on in Section 3.3.1, before the impact on redox reaction rates is highlighted in Section 3.3.2.

3.3.1. Oxygen transport capacity of OC

To assess the oxygen transport capacity of the OC samples, its weight change inside the TGA was assessed over five redox cycles (more details see Section 2.4.5). Here it was found that all samples exhibit stable oxygen transport capacities over five cycles, ¹⁰ thus signifying the oxygen transport capacity of the OC materials inside the 1 MW_{th} CLG unit.

When considering the progression of the oxygen carrying capacity of the OC (ROC) over time, Fig. 10 shows that it decreases visibly during CLG operation. While R_{OC} values close to that of fresh ilmenite were determined for LS samples collected shortly after the start of chemical looping operation (K1: 10th April 2022, K2: 21st June 2022), the oxygen transport capacity of the OC decreased to below 3 % for K1 within four days of operation, despite continuous make-up feeding. A similar behavior was observed during redox cycling in different setups [26,27], with the OC's oxygen carrying capacity decreasing continuously over up to 100 cycles [27]. This behavior was attributed to the formation of Fe₂O₃ at the expense of Fe₂TiO₅ inside the OC particle during redox cycling, with the former exhibiting a lower oxygen transport capacity than the latter [27]. This change in particle chemistry can be related to the compositional changes taking place inside the OC during chemical looping operation, i.e. the iron migration inside OC particles (more details see Section 3.1). Another factor contributing to the decreasing R_{OC} with time, is the abrasion of the Fe-rich outer layer of the OC particles (see Section 3.1), leading to a selective removal of the active OC phase from the system. For K2, stable R_{OC} values in the range of 2.7–3.2 % were obtained after approx. five days of chemical looping operation, showing that in case of continuous make-up feeding, the oxygen transport capacity of the OC inside the CLG system stabilizes if sufficiently

⁹ One such option, which has been successfully utilized in DFBG units, is the separation of particles in a filter equipped with an automatic recycling route back to the gasifier, to reduce fresh material consumption and convert entrained char [54,55]. Another viable approach would be the utilization of a widened U-turn in a vertically-aligned two-stage gas cooler, in which particles settle down and can then be removed (e.g. via a rotary valve) and recycled. Alternatively, a second cyclone could be used to enhance the overall solid separation from the gas stream.

 $^{^{10}}$ Selected samples were analyzed for up to 50 cycles, exhibiting stable R_{OC} values for the entire TGA experiment.

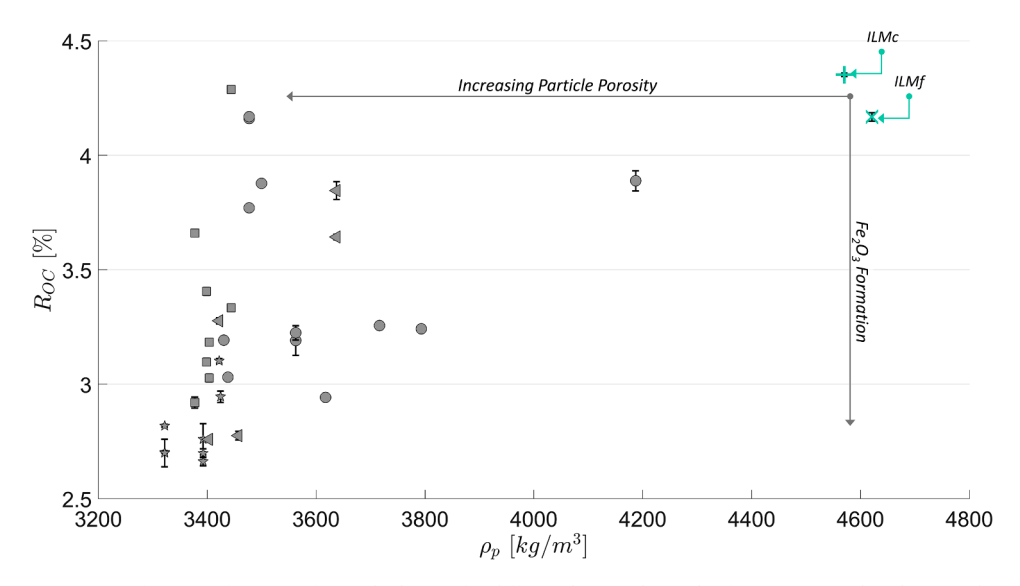


Fig. 11. Oxygen transport capacity of OC as a function of particle density for different loop seal samples from 1 MW_{th} pilot plant (circles: K1, triangles: K2-ILMc, pentagrams: K2-ILMf, squares – K3). Values for fresh OC materials are given as a reference (plus: ILMc, cross: ILMf).

long operation durations are provided.

While this decrease in R_{OC} is of great relevance for CLC operation, where high oxygen transport rates to the FR are essential for process efficiency [24,27], it does not pose a major issue for CLG operation, where oxygen transport from the FR to the AR has to be restricted to maximize process efficiency [16,52]. With minimum values of approx. 2.6 % being determined for R_{OC} for samples collected from the 1 MW_{th} CLG unit, it can thus be summarized that the observed decrease in oxygen transport capacity does not pose a critical issue for operation, as oxygen fluxes up to 365 kg/h would still be obtainable in the 1 MW_{th} unit. This oxygen release would yield a maximum attainable oxygen-to-fuel equivalence ratio of 0.87, well above λ =0.3–0.35, required for autothermal CLG operation [52,57], meaning that even for lower values of R_{OC} oxygen release by the OC inside the FR would still need to be limited via process control [52].

Fig. 11 relates the particle density of the OC, giving an indication of the physical changes it has undergone (see Section 3.2), with the oxygen transport capacity of the OC sample, signifying its chemical ageing. Here it becomes obvious that while the density of the majority of OC particles lies within a relatively narrow range of 3300 to 3700 kg/m³ (fresh OC: 4600 kg/m³), the variation in R_{OC} is much bigger, ranging from 2.5 to 4.0 % (fresh OC: 4.2 %). This finding suggests that the increase in particle porosity because of thermal, mechanical, and chemical strain inside the CLG is a comparably fast process, yielding particle densities <3700 kg/m³ within a few hours. On the other hand, the chemical ageing of the OC inside the CLG unit seems to occur over a longer duration, leading to decreasing R_{OC} values with each redox cycle. Another interesting finding which can be inferred from Fig. 11 is that the lowest oxygen transport capacities were obtained when fine ilmenite was used during K2 (pentagrams in Fig. 11). For this operational period, the cold gas efficiency of the CLG unit was maximized by restricting the oxygen transport to the FR. This approach thus led to the OC being highly reduced in the FR [29, 581, i.e. the chemical strain on the OC was intensified. This explains why lower oxygen transport capacities were obtained for this operational period, as it is established, that iron migration to the OC surface is accelerated in more reducing environments [28].

3.3.2. Redox reaction rates of OC

In contrast to the oxygen carrying capacity of the OC, its oxygen release rate plays a crucial role in CLG, determining how deeply the OC is reduced inside the FR [29,52]. The shrinking core model, widely used to describe the oxygen release by the OC inside the chemical looping system in literature [59,60], states the oxygen release rate of the OC decreases with decreasing R_{OC} , since the OC's propensity to release oxygen decreases at it is further reduced. However, Adanez et al. [27] found that contrary to this explanation, stable OC oxygen release rates can be observed during redox cycling. This was attributed to the increase in particle porosity incurring during redox cycling (see also Section 3.1), enhancing the oxygen release of the OC and hence countering the negative effect of decreasing R_{OC} values on redox kinetics. To assess to which extent oxygen release and uptake rates of the OC change during redox cycling inside the 1 MWth CLG system, the rate index of different loop seal samples collected during operation were determined via TGA (see Section 2.4.5). The reduction rate indices (RI_{red}) determined for the OC samples for the reduction step are shown in Fig. 12a.1-c.1. Upon consideration of the data, the following observations can be made:

- The reduction rates for the fresh OC remain relatively constant for each redox cycle, confirming findings made by Adanez et al. [27];
- On the other hand, the reduction rates of the utilized OC samples decrease from the first to the third redox cycle, before reaching a relatively stable value from the fourth cycle onwards;¹³
- For the first TGA cycle, used OC samples exhibit significantly higher reduction rates than the fresh OC material;
- For the fifth redox cycle, reduction rates of the utilized samples lie within the range of the reduction rates of the fresh OC material (2.5–4.5 wt.-%/min). These reduction rates are similar to values reported in literature [27].

When considering the first redox cycle (see Fig. 12a.1), where the OC samples still exhibit the same characteristics as in the 1 MW $_{th}$ unit, the high reduction rates when compared to the fresh OC underline that oxygen release kinetics in the FR are not deteriorating during CLG operation. This can be explained by the increased particle porosity of the

 $^{^{11}}$ Assuming an OC circulation rate of 14 t/h.

 $^{^{12}}$ For a thermal load of 1.2 MW $_{
m th}$ (industrial wood pellets as the feedstock) and assuming full reduction and oxidation of the OC inside the FR and AR, respectively.

¹³ By investigating different samples for 25 redox cycles inside the TGA, it was found that rate indices reach an entirely constant value after 7-10 TGA redox cycles, with samples exhibiting a sharper decrease in reaction rates during the first three cycles requiring more cycles for stabilization.

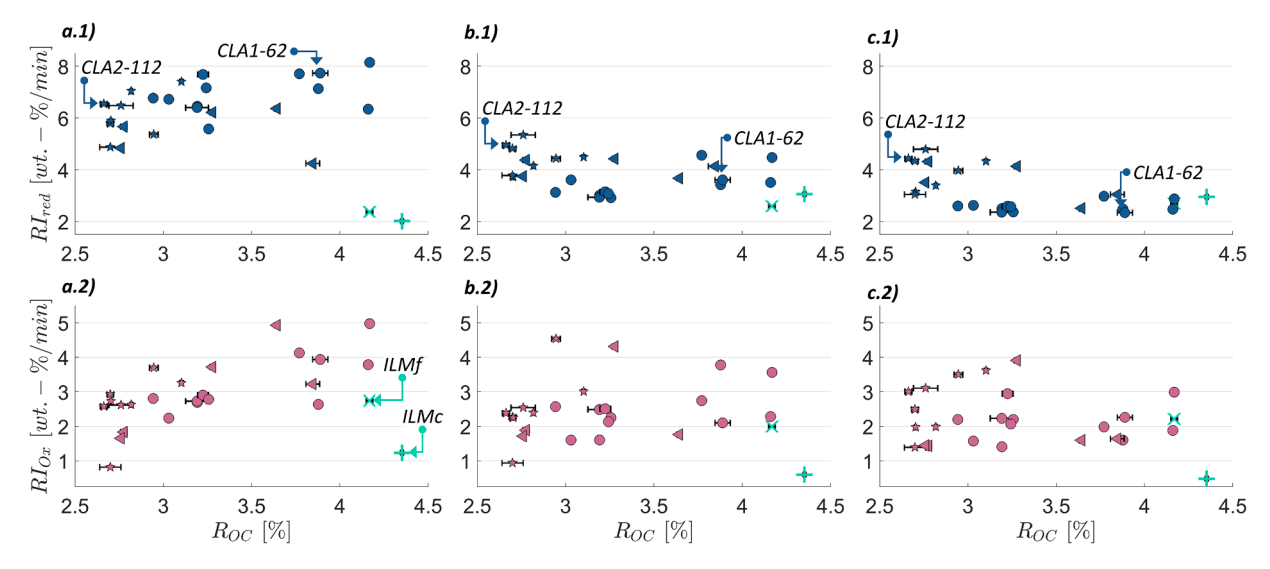


Fig. 12. Reduction (1) and oxidation (2) rate index for different loop seal samples from 1 MW_{th} pilot plant for first (a), third (b) and fifth (c) TGA cycle, (circles: K1, triangles: K2-ILMc, pentagrams: K2-ILMf). Values for fresh OC materials are given as a reference (plus: ILMc, cross: ILMf).

utilized OC samples, induced through thermal, chemical, and mechanical strain (see also Section 3.2.2). Overall, the data from the first redox cycle in the TGA thus suggests that the effect of increased particle porosity on oxygen release rates dominates the effect of decreasing oxygen transport capacities for the OC samples from the 1 MW_{th} unit, thus leading to larger RI_{red} values for the utilized materials than those of the fresh OC material. Moreover, the highest oxygen release rates are obtained for utilized OC samples exhibiting relatively high R_{OC} values (>3.0 %). This again supports the hypothesis that mechanical ageing of the OC particles inside the CLG unit is a faster process than chemical ageing (see also Section 3.3.1). This means that particles located inside the system for several hours still exhibit a comparably high oxygen transport capacity, as iron migration to the surface has only occurred to limited extents, yet their porosity has already increased substantially. This consequently leads to high rate indices (>7 wt.-%/min) for those samples.

To explain why the rate indices of the utilized OC materials decrease during redox cycling inside the TGA, the differences between different samples provide insights into potential mechanics of the occurring processes. As the fresh OC materials do not exhibit a decrease in reduction rate indices during redox cycling (see Fig. 12a.1-c.1), it can be postulated that a characteristic of the utilized OC particles crucial for oxygen release rates is altered during TGA cycling. As R_{OC} values remain unchanged for all samples for each TGA cycle (see Section 3.3.1), it can thus be presumed that the particle porosity of the utilized OC materials is decreased with each TGA cycle. Here, one hypothesis is that in the absence of mechanical and thermal stress inside the TGA, small cracks and defects formed because of those strains inside the 1 MWth CLG unit, are "healed" as oxygen migrates through the lattice structure, leading to its restructuring. ¹⁴ Another hypothesis is that the surface of the OC is restructured during oxidation inside the TGA, owing to the strongly exothermic reaction and ensuing high surface temperatures. These hypotheses would also explain why the extent of decrease in reduction rate indices with each cycle varies between different OC samples. While for samples with high R_{OC} values (indicating minor chemical ageing), a drop

in *RI_{red}* values by more than two thirds can be observed (see sample CLA1–62 in Fig. 12a.1–c.1), the decrease is more moderate for samples with lower oxygen transport capacities (see sample CLA2–112 in Fig. 12a.1–c.1). This means that the observed restructuring occurs more pronouncedly inside the TGA for OC samples exhibiting only minor defects induced through short-term mechanical and thermal strain (CLA1–62), whereas larger defects arisen through longer CLG durations cannot be healed to the same extent inside the TGA (CLA2–112). By investigating selected samples after 1, 2, 4, and 8 TGA cycles via SEM, it was validated that porosity in the particle bulk, the distribution of Iron and Titanium along the particle diameter, as well as the morphology of the OC surface change with increasing cycling duration inside the TGA. This shows that TGA cycling changes OC properties. Thus, the rate indices measured during the first TGA cycle are representing the state of the OC inside the CLG system most accurately.

Consideration of the rate indices determined for the oxidation step, shown in Fig. 12a.2–c.2, shows that the utilized OC samples exhibit similar oxidation rates as the fresh OC material. In contrast to the reduction step, distinct impacts in terms of OC particle properties or TGA cycle number on oxidation rate indices cannot be observed. This suggests that due to the relatively high partial pressure of oxygen used inside the TGA (0.21 atm), leading to fast oxygen take-up rates by the OC, other factors (e.g. bulk diffusion) govern the oxidation kinetics for the given boundary conditions.

All in all, these results show that TGA redox cycling affects OC properties differently than redox cycling in a real chemical looping setup. Depending on the state of the sample used inside the TGA and the boundary conditions used during redox cycling, the incurring effects on particle morphology and composition vary. Hence, TGA studies provide fundamental insights into the general mechanics of the impact on redox cycling on OC particle characteristics, yet do not provide a holistic picture of the chemical properties of the OC inside a CLG system, e.g. due to the absence of mechanical and thermal stresses inside a TGA setup. Nonetheless, TGA studies can be utilized to assess the redox behavior of OC samples. In the current study, the utilized OC samples were found to exhibit a higher reduction rate than the fresh material, which was attributed to the changes in morphology the OC undergoes during chemical looping operation. On the other hand, oxidation rates were found to be unaffected by OC morphology, indicating a kinetic limitation independent of particle morphology (e.g. bulk diffusion).

3.3.3. Summary

Thermogravimetric analysis of loop seal samples collected during 1

 $^{^{14}}$ The absence of any decreasing trend of R_{OC} even during long-term redox cycling inside the TGA (50 cycles), also indicates that in contrast to other studies [27], the redox conditions used for TGA cycling in this study did not promote any major changes in chemical composition of the OC. This shows that due to the moderate redox conditions used inside the TGA, the OC was given sufficiently long times for homogeneous chemical restructuring.

 $\mathrm{MW_{th}}$ operation revealed that changes in the OC chemistry, induced through redox cycling (see Section 3.1), lead to a reduction in the OC's ability to transport oxygen from the AR to the FR. However, this drop-off in R_{OC} is not crucial for CLG operation, where oxygen transport to the FR is of lesser importance than the heat transport facilitated by the circulating OC [52,57]. Additionally, it was shown that oxygen uptake and release rates of the utilized OC are generally higher than those of fresh, activated ilmenite. This was attributed to the increase in particle porosity the OC incurs during redox cycling inside the CLG system. Consequently, the chemical properties of the OC do not determine the lifetime of the OC inside the 1 MW_{th} CLG system, which means that generally, replacement of the OC inventory via sluicing from the reactor system was not required. Hence, it can be inferred that active OC replacement due to chemical deactivation should also not be necessary in an industrial CLG unit.

3.4. Effect of feedstock properties on OC during 1 MWth pilot testing

In terms of feedstock interactions, ilmenite is known to be an attractive oxygen carrier, which is not prone to excessive feedstockrelated carbon deposition or deactivation phenomena [26]. These findings were validated in 1 MWth pilot scale, as the utilized ilmenite materials did not exhibit any significant deactivation phenomena, indicating blocking or poisoning of active sites for any of the three utilized feedstocks (see also Section 3.3). However, these properties do not prevent operational issues related to the combination of high reactor temperatures and potential low-melting ash components in biomass chemical looping. While these are of lower importance for woody biomasses, generally exhibiting low ash contents and ashes with sufficiently high melting points, it becomes a relevant issue for herbaceous or agricultural biomasses (e.g. rice husk or wheat straw) [61]. Apart from the higher ash content of these biomasses, this can be related to their ash chemistry, rich in silicates and alkali salts [61], which are known to increase the risk of formation of low-melting eutectic phases [38,62,63].

These general findings regarding ash melting were also observed during pilot testing in 1 MW_{th} pilot scale. While agglomeration was not observed to any extent during CLG operation with the woody feedstocks IWP and PFR, excessive agglomeration was detected during CLG

operation with WSP in K3, within a single day of chemical looping operation (see Fig. 13). Maintaining fluidization in both reactors despite the occurrence of agglomeration was not an issue. However, the continuous growth of the OC particles led to a decrease in entrainment from both reactors, which is an issue also discussed in literature [64]. With the decrease in entrainment rates from both reactors, OC circulation rates dropped, leading to increasing temperature differences (ΔT) between AR and FR with increased operating time, as less heat was transported between AR and FR by the OC, ultimately leading to low CLG process efficiencies [58]:

$$\dot{Q}_{OC} = \dot{m}_{OC} \cdot c_{p,OC} \cdot (T_{AR} - T_{FR}) = \dot{m}_{OC} \cdot c_{p,OC} \cdot \Delta T \tag{8}$$

This underlines, that the pronounced occurrence of feedstock related agglomeration poses an issue requiring further attention when striving for the upscaling of the CLG technology. The observed operational issues are of an increased concern as the WSP used during K3 were pre-treated, using a pre-treatment concept developed using different modeling and experimental techniques [36,39,65], which led to stable CLG operation with wheat straw pellets in 20 kW_{th} scale [14]. This poses the question why agglomeration occurred inside the 1 MW_{th} pilot to the observed extents. In the following sections it will thus be attempted to provide an explanation for the observed behavior by providing insights gathered during inspection of the CLG unit after operation with WSP (Section 3.4.1), further analysis of the raw materials used during pilot testing (Section 3.4.2), and subsequent analysis of samples collected during pilot testing (Section 3.4.3). Finally, a summary of the results and a strategy to prevent this behavior are presented in Section 3.4.4.

3.4.1. Inspection of 1 MW_{th} CLG unit after operation with WSP

Subsequent to the shut-down of the CLG unit after K3, all relevant components of the cooled-down 1 MW_{th} pilot plant were inspected, to be able to locate the main reaction regions in which agglomeration had occurred during CLG operation (more details see Table A 1 in the Supplementary Material). Here, it was found that the majority of agglomerates as well as the agglomerates with the greatest dimensions were found inside the AR, which is illustrated in Fig. 14. Interestingly, very large zones of coherent agglomerates were recovered towards the top of the AR riser, as well as the AR cyclone, and LS1 incl. its standpipe.



Fig. 13. Images of OC at start of experiment (left), during CLC operation (28th Aug.) and CLG operation (29th August).

Images of those agglomerates are shown in the insets in Fig. 14.¹⁵ Upon closer inspection of the removed parts, it was noticed that the slabs exhibit a layered, porous structure, suggesting that they had been formed continuously over time. Moreover, the retrieved junks exhibited certain mechanical stability despite their porosity, yet could be broken down manually, without the need of additional tools, due to their brittleness (see Fig. 15).

On the FR side of the CLG unit (i.e. FR and LS5), only small agglomerates were found (located on the nozzle grid of the FR and LS5), suggesting that agglomeration did not occur to substantial extents inside the FR. Therefore, it can be postulated that in the 1 MW_{th} pilot agglomeration was mainly driven by temperature (being higher inside the AR) and not by reaction atmosphere, which are both known to play a critical role in agglomeration phenomena¹⁶ [61]. Moreover, it can be assumed that as the feedstock pellets entered the AR and were fully converted with the inlet oxygen. This resulted in particles solely consisting of ash components, also favoring the occurrence of ash melting and ultimately agglomeration. When considering the reactor locations from which large agglomerates were retrieved, it becomes obvious that these exhibit zones where the following conditions were met during CLG operation:

- Temperatures > 900°C,
- · Oxidizing atmosphere, leading to full char conversion,
- Low gas velocity/low turbulence.

Consequently, it is postulated that in zones exhibiting low turbulence, molten ash particles, formed at hot and oxidizing conditions inside the AR according to the melt-induced agglomeration mechanism [61,66], were able to stick to the reactor lining (see Fig. 16c). Subsequently, the circulating oxygen carrier adhered to this sticky surface (Fig. 16d), leading to a steady growth in the size of the agglomerated layer (Fig. 16e) until the fully formed slab was continuously formed (Fig. 16d). Growth of the slab into more central zones of the AR riser, where gas velocities and gas solid loadings are higher, was prevented by attrition through the by-passing OC particles, removing protruding parts. Following a similar mechanism (i.e. via molten ash particles forming inside the AR), smaller agglomerates were formed inside the AR, as OC particles collided with the molten ash. Yet, in contrast to the larger agglomerate slabs, these agglomerates were maintained in a fluidized state inside the fluidized bed, preventing their continuous growth via attrition (see also Fig. 24). Hence, smaller particle agglomerates could be recovered from the AR via ash sluicing.

While the proposed mechanism, illustrated in Fig. 16, explains the formation of agglomerates retrieved from the AR during operation and inspection of the CLG unit, the root cause for the occurrence of agglomeration inside the 1 MW_{th} pilot plant, whereas stable long-term operation without observation of any agglomerates was feasible for pre-treated wheat straw pellets in the 20 kW_{th} scale [14,48], remains unclear. In order to answer this question, an in-depth analysis of the fresh materials utilized during 1 MW_{th} pilot testing (Section 3.4.2) as well as of samples collected from different parts of the CLG unit during operation and inspection (Section 3.4.3), was carried out and is presented below.

3.4.2. Characterization of fresh materials utilized during 1 MW_{th} CLG operation with WSP

In a first attempt to explain why agglomeration had occurred during 1 MWth pilot testing in the observed extent, the fresh materials were analyzed to assess whether it is possible to predict the agglomerating tendency of the feedstock. For one, the ash of the pre-treated wheat straw pellets was analyzed regarding its elemental composition. Based on the resulting data (see Table A 6 in the Supplementary Material), the ash melting behavior of the wheat straw pellets was modelled using the software FactSage, via the approach detailed by Lebendig et al. [38]. As shown in Fig. 17, it was found that the pre-treated wheat straw pellets (WSP) used during 1 MWth pilot testing generally exhibit a significantly higher melt fraction than the other two feedstocks used during pilot testing. At the maximum AR temperature experienced during K3 (1025°C), WSP exhibit almost 80 wt.-% slag content, indicating pronounced melt formation at the relevant reactor temperatures, whereas IWP and PFR only exhibit 30 and 18 wt.-%, respectively. For comparison, the pre-treated additivated wheat straw pellets used during CLG operation in 20 kWth scale by Condori et al. [14] are also shown in Fig. 17, displaying a slag amount approx. 20 wt.-% lower than that of WSP at this temperature. Another factor probably having prevented extensive slag formation during 20 kW_{th} testing is the absence of a significant temperature difference between AR and FR for externally heated units (more details see Section 3.2.1), generally leading to lower AR temperatures in the 20 kWth setup.

These findings were validated by hot stage microscopy (see Section 2.4.7), showing that ash melting commences at 920°C and intensifies around 1000°C for the WSP, whereas IWP and PFR feedstock used during K1 and K2 do not show any signs of deformation before 1200°C (see Fig. 18). This behavior can be related to the relatively high amount of K and a relatively low amount of Si present in the ashes of the WSP, which can be considered to be a first indicator for a lower melting point (more details see Section A.2.1 in the Supplementary Material).

To further assess the agglomeration tendency of the WSP with the two utilized ilmenite types (coarse: ILMc & fine: ILMf) in a relevant environment (i.e. a fluidized bed), their fluidizing behavior in N2 at temperatures between 700 and 1000°C was investigated (see Section 2.4.6). Through this approach, previously used to determine the suitability of different feedstocks for CLG [35], it was assessed whether the agglomerating behavior of the raw materials used during 1 MWth pilot testing could be replicated in a lab setup. It was found that in terms of the fluidization behavior, the presence of WSP-ashes did not significantly alter the fluidization behavior of the two utilized ilmenite types (more details see Section A.2.2 in the Supplementary Material). 17 However, subsequent SEM analysis of the tested samples showed agglomeration had occurred to some extent inside the fluidized bed quartz reactor (see Fig. 19, more details see Section A.2.3 in the Supplementary Material). Therefore, it can be concluded that similar melting phenomena also occurred in the 1 MW_{th} pilot. Hence, it can be postulated that the combination of the significantly longer duration of

 $^{^{15}}$ For removal of the agglomerates from the reactor system, they had to be manually crushed to the smaller pieces shown in Fig. 14.

¹⁶ Generally, it is know that ash melting occurs earlier (i.e. at lower temperatures) in reducing atmospheres [61]. As only minor amounts of agglomerates were retrieved from the FR, it can be concluded that FR temperatures were too low to lead to ash melting, despite the fact that a reducing atmosphere was present.

 $^{^{17}}$ Although the utilized ilmenite did not exhibit any fluidization issues inside the 1 MW_{th} unit, neither during CLG pilot testing nor in previous CLC test campaigns, the laboratory-scale evaluations by Pressure Fluctuation Tests of the ILMf and ILMc samples investigated in this work showed that both samples develop some recalcitrance towards fluidization at the high temperatures (>900 °C), identified by the overpressure peaks preceding fluidization in "pressure drop vs. superficial velocity" experimental curves (not shown). This behavior occurred more pronouncedly for ILMf, with the extreme consequence of the absence of its bubbling fluidization at 1000 °C, whereas ILMc remained fluidizable by bubbling fluidization also at 1000° C. The development of more pronounced adhesion forces between finer particles and with quartz reactor walls is a possible explanation. Other coarse ilmenite samples, previously studied by the same method elsewhere [35–37], usually showed bubbling fluidization in the presence of ashes at three times their minimum bubbling velocity.

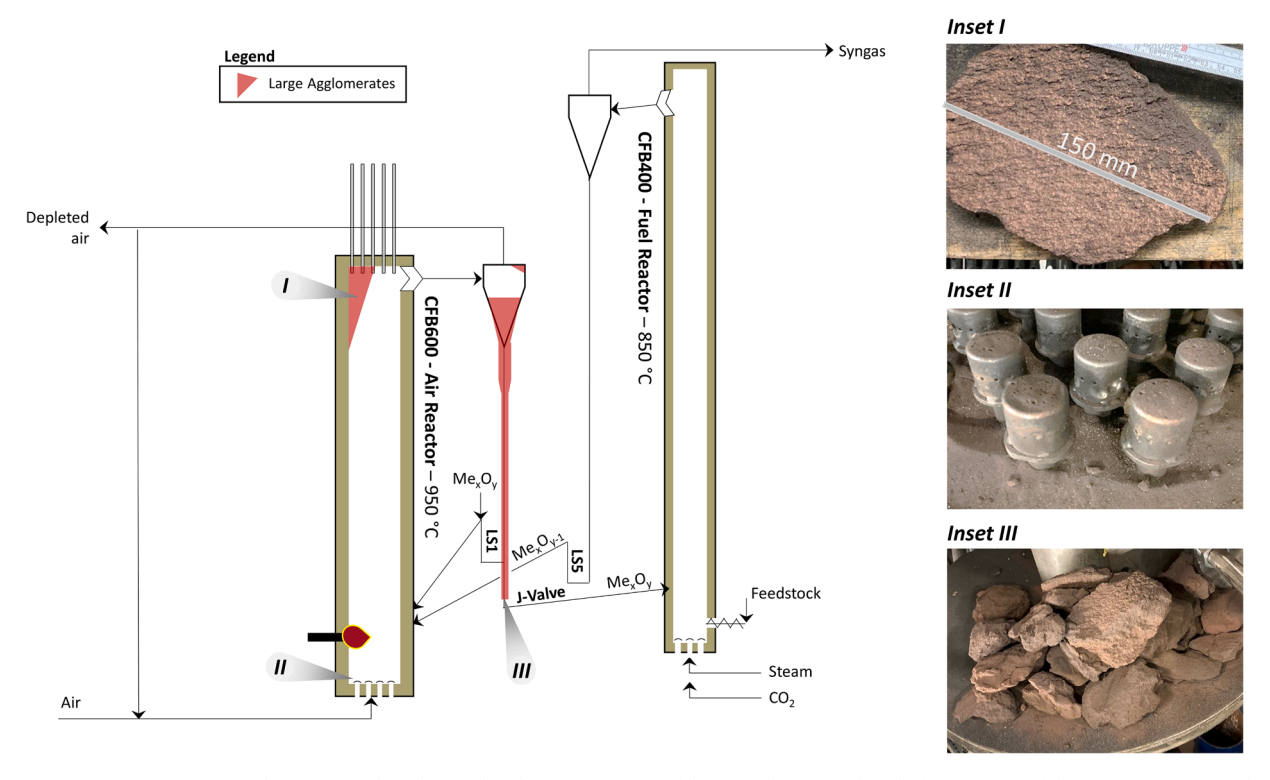


Fig. 14. Layout of reactor system of the 1 MW_{th} pilot plant with indication of zones of large agglomerates found after opening of the reactor. Insets: Agglomerates found in riser (Inset I), on nozzle grid (Inset II) and in stand-pipe of LS1 (Inset III).

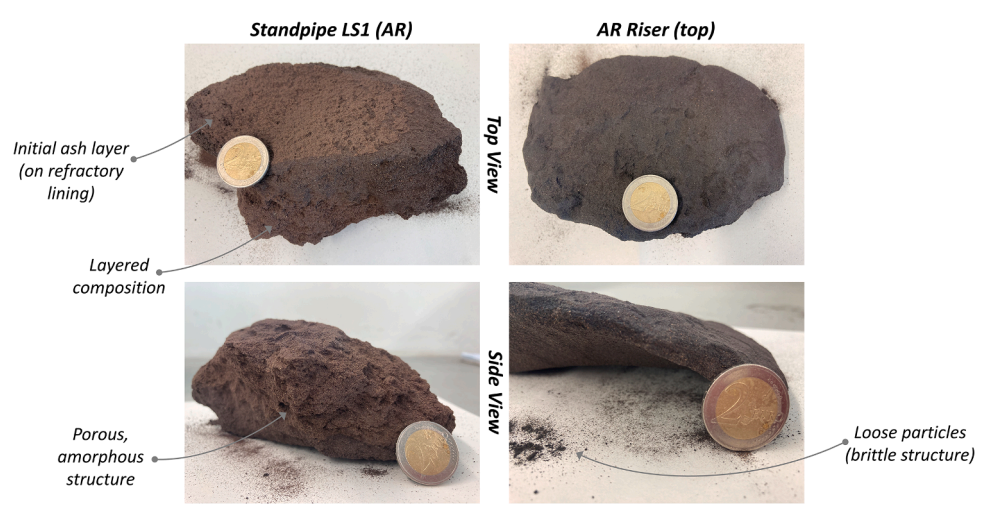


Fig. 15. Close-up images of large agglomerate slabs collected from the standpipe of LS1 (left) and AR riser (right).

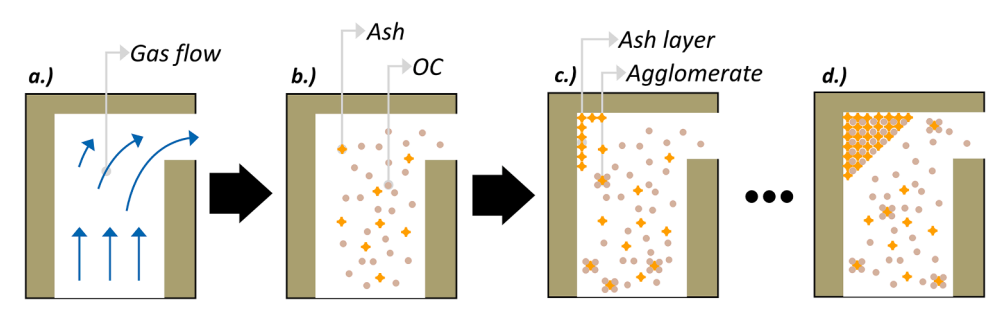


Fig. 16. Postulated mechanism for formation of large agglomerate slags inside AR: a.) Empty AR with indication of gas flow, b.) AR with ilmenite and ash particles, c.) formation of first agglomerates and sticky ash layer on AR refractory lining in zones of low turbulence & adherence of ilmenite particles on ash layer, d.) growth of ash/OC layer on refractory lining, yielding fully formed agglomerate slabs.

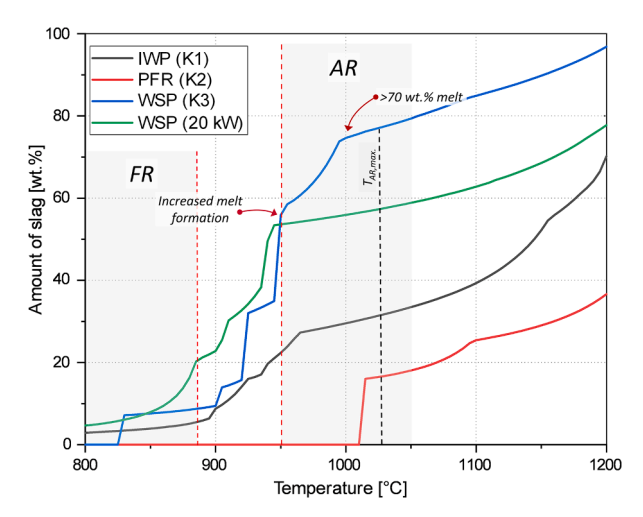


Fig. 17. Modelled melt fraction of selected feedstock ashes considering all major ash components. Grey shaded areas denote the FR and AR temperature range experienced in the 1 MW_{th} pilot plant.

the pilot experiments and the exposure of the OC bed material to more feedstock ashes inside the 1 MW $_{th}$ CLG unit consequently led to the formation of larger agglomerates inside the reactor system, leading to an increase in the average particle size of the OC as well as the formation of large agglomerates in zones of low turbulence.

3.4.3. Characterization of different samples collected during 1 MW_{th} CLG operation with WSP

After determining that agglomeration also occurs in lab-scale setups and hence must be related to the properties of the raw materials, rather than the setup of the 1 MW $_{th}$ pilot plant, samples collected during 1 MW $_{th}$ CLG testing were analyzed to obtain a better understanding of the occurring mechanism. These samples included samples collected from the six sampling locations of the 1 MW $_{th}$ pilot plant (see Fig. 2) during

pilot testing, as well as samples collected from the pilot during inspection after plant shut-down (see Fig. 14).

The solid samples collected during operation were analyzed via SEM-EDX and their particle size distributions were determined to quantify the extent to which agglomeration had occurred.

Upon consideration of Fig. 20, it can be postulated that agglomeration had already started to occur shortly after the start of CLC operation, as particles with diameters larger than 350 µm were recovered from the loop seals and bottom ash (K3). Clearly, those particles cannot stem from the fresh OC materials, exhibiting maximum particle diameters of 300 μm. Moreover, the PSD of the loop seal samples from K3, is clearly shifted towards the right when compared to K1 and K2, evidencing the occurrence of agglomeration during operation with wheat straw pellets. Upon consideration of the PSD from the AR bed material collected during CLG operation in K3 (see Fig. 20), it can be seen that the coarse fraction of the OC inside the riser of the AR exceeds that found inside the loop seals. Hence, it cannot only be summarized that agglomeration had occurred, but also that due to this, the formed agglomerates accumulated at their origin (AR) and only partially participated in OC circulation. That means, the formed agglomerates can be expected to reduce the attainable global solid circulation of the CLG system, as their entrainment is significantly lower than for the raw OC [64]. Still, judging from the recorded PSDs shown in Fig. 20, some agglomerates $(d_p>300 \mu m)$ were also recovered from both loop seals, meaning that they are either transported there from their origin of formation or that agglomerates form inside the cyclones/stand-pipes before accumulating inside the loop seals. When considering the observations made during inspection of the pilot plant subsequent to CLG operation (see Section 3.4.1), the former hypothesis seems to be the more convincing one for LS5, as the AR and LS1 were found to be the main origin for agglomerates, yet particles larger 350 µm are recovered in LS5. Due to the high temperatures present in LS1, it can be assumed that agglomeration also occurred between the AR outlet and LS1 (see also Section 3.4.1). This is also validated by Fig. 20 showing that more agglomerates were found inside LS1 than in LS5. Consequently, it can be summarized that agglomerated particles with diameters up to 400 µm still participated in

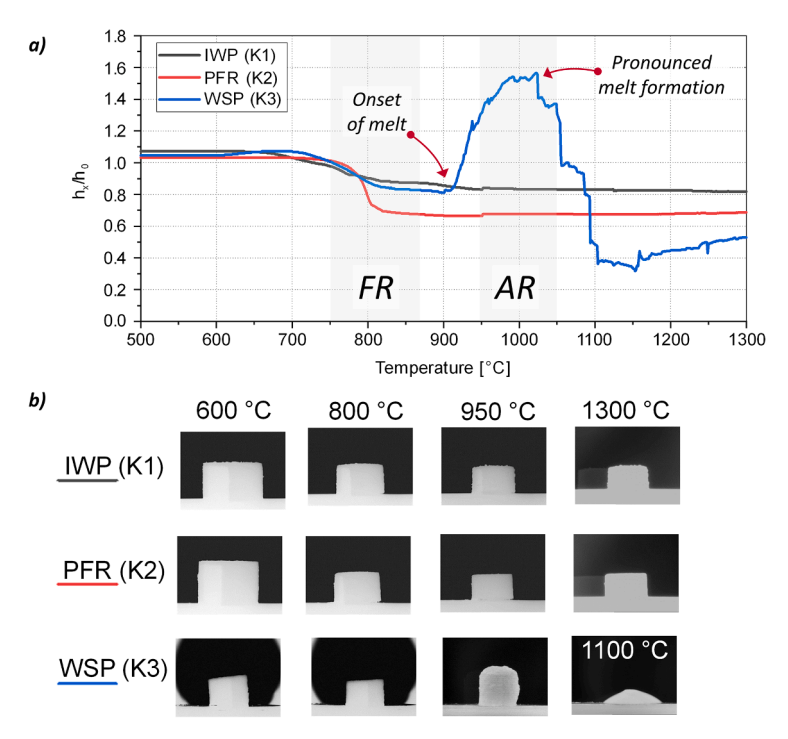


Fig. 18. Sintering and melting behavior of selected feedstock ashes investigated by hot stage microscopy. a.) Change in relative height during hot stage microscopy. Grey shaded areas denote the FR and AR temperature range experienced in the 1 MW_{th} pilot plant. b.) Images of ash samples recorded during hot stage microscopy for selected temperatures. Results for IWP and PFR adapted from [38].

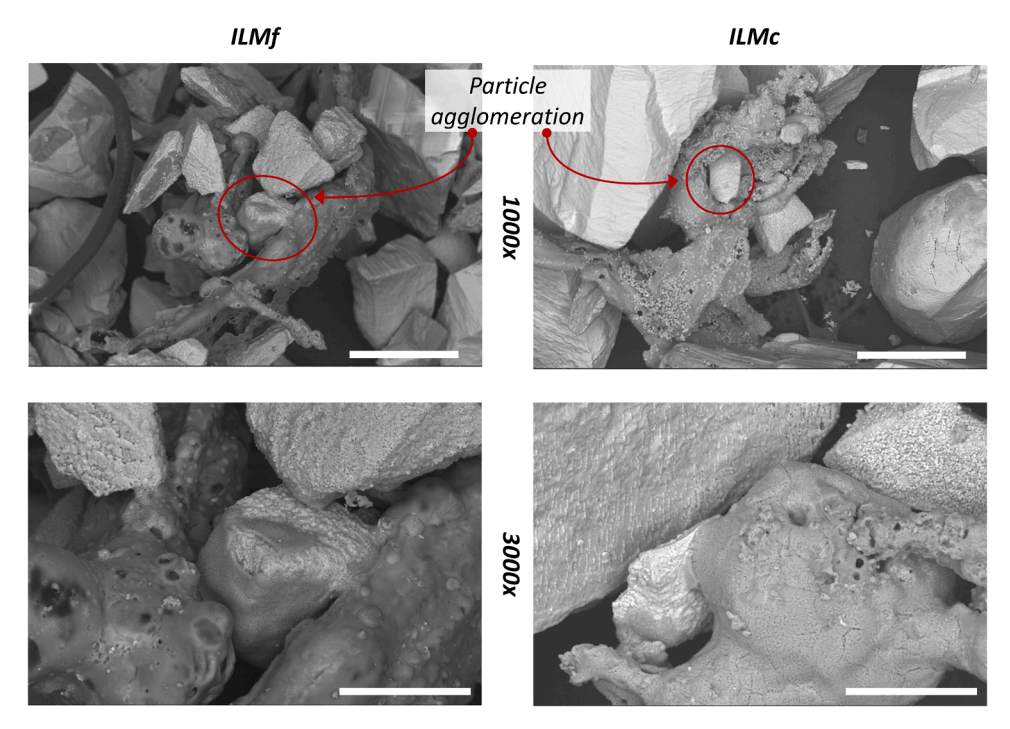


Fig. 19. SEM micrographs of ILMf+WSP-ash (left) and of ILMc+WSP-ash (right) after fluidization with N_2 at 1000° C, magnified at: 1000x (top) and 3000x (bottom). Red circles indicate detection of particle agglomeration. The white bar denotes a length of $100 \mu m$ (top) and $40 \mu m$ (bottom).

solid circulation, leading to their dispersal in the entire CLG unit, yet due to their impaired mobility inside the CLG system, they accumulated at their origin of formation. Apart from the agglomerate-related effects, the PSDs of materials sampled from the 1 MW_{th} pilot plant, shows similar trends as for K1, with the fine fraction of the OC being recovered in the AR and FR filter (more details see Section 3.2).

When considering the PSDs for the bed material samples collected from the AR (i.e. at the postulated source of the found agglomerates) for different operating times, further information on the progression of agglomeration formation inside the 1 MW $_{th}$ CLG unit can be derived. Shortly after completion of system start up (= termination of OC-aided combustion operation at 0 h), the PSD still largely resembled the PSD of

coarse ilmenite, used during this operational period (see 5 h in Fig. 21). This indicates that agglomeration had not occurred to substantial extents before initiating chemical looping operation. Subsequently, the coarse ilmenite inside the CLG system was slowly replaced with fresh fine ilmenite between 5 h and 24 h, as chemical looping operation was commenced and boundary conditions were optimized. However, despite this bed material replacement, which should have entailed a drop in OC particle sizes, the average PSD inside the AR clearly shifted to the right, with particles ${>}350~\mu{\rm m}$ making up more than 25 wt.-% of the AR inventory and the median particle diameter increasing to 235 ${\mu{\rm m}}$ after 24 h chemical looping operation. The only viable explanation for this observation is that the pronounced occurrence of agglomeration inside

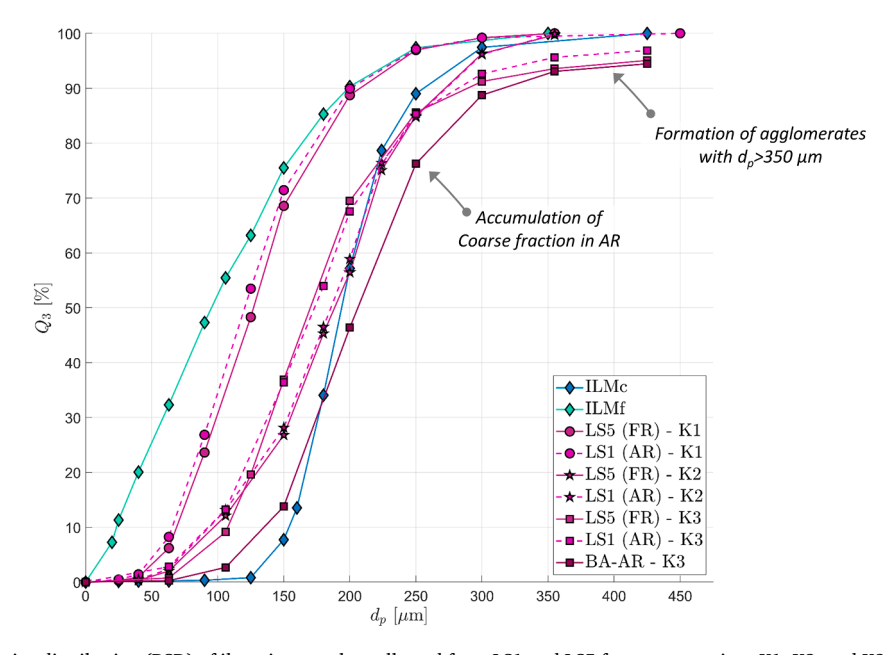


Fig. 20. Cumulative particle size distribution (PSD) of ilmenite samples collected from LS1 and LS5 for test campaigns K1, K2, and K3. PSD of fresh OC materials are given as a reference.

the AR during chemical looping operation. As the used ilmenite inside the system was replaced with fresh fine ilmenite to large extents after agglomeration was detected by the plant operators between 50 and 55 h, the PSD of the AR clearly shifted to smaller particle diameters. This intervention led to significantly improved system hydrodynamics as the average particle size of the OC decreased, allowing for larger solid circulation rates between AR and FR [46]. However, as shown in Fig. 21, the positive effect was short-lived, as the PSD subsequently deteriorated dramatically from 55 h over 89 h and 90 h, until the median particle diameter inside the AR reached 560 μ m before system shut down (93 h).

The findings made via PSD analysis are also supported when considering the SEM images of loop seal samples from K1 and K3, shown in Fig. 22. While for K1, the most notable observation is the change in shape of the OC particles to a more round form, which can mainly be attributed to abrasion [67,68] (see also Section 3.3), samples from K3 clearly show large agglomerates composed of multiple OC particles. Moreover, visibly more agglomerates are found in LS1 than in LS5, supporting the hypothesis that the AR is the origin of the agglomerates and those large particles are only found in LS5 after entrainment form the AR and FR. In terms of the formation mechanism of the agglomerates, the SEM image for K3 in LS1 shows agglomerates of multiple sizes, supporting the hypothesis, illustrated in Fig. 16, that molten WSP ash functions as a glue binding particles and agglomerates together, according to the melt-induced agglomeration mechanism, which was found to be dominant in chemical looping systems [61], thereby leading to an increase in particle size with increasing operating time.

Further analysis of a sub-set of solid samples collected after shutdown of the CLG unit (see Table A 2 and Figure A 4 in the Supplementary Material) was carried out to explain the formation of agglomerates in the cm-range (see Section 3.4.1). These samples were analyzed via EDXRF and XRD analysis, thereby determining elemental and mineral composition, respectively, as well as via SEM-EDX. SEM-EDX analysis showed that the agglomerates retrieved from the air reactor (CLA-S-75, photograph see Fig. 23a) consist of individually distinguishable particles sticking together (see Fig. 23b,c and Figure A 5 and in the

Supplementary Material), supporting previous findings. By means of EDX analysis, these agglomerated particles were identified as oxygen carrier material (mainly consisting of Ti, Fe and O) and ash particles (mainly consisting of Si, K, Ca and O). As indicated by the chemical analysis, the samples contain a high amount of the oxygen carrier ilmenite, which not only consists of the mineral phase Ilmenite (FeTiO₃) but also Hematite (Fe₂O₃) and Pseudobrookite (Fe₂TiO₅). The latter two phases contain Fe³⁺, indicating that the oxygen carrier was - even inside the FR - far from being completely reduced. Furthermore, Titanite (CaTi (SiO₄)O) and Hollandite (K_{1.5}Ti_{7.2}Fe_{0.8}O₁₆) are present inside the samples, which are both reaction products of ilmenite and ash, indicating a certain chemical interaction between the WSP ashes and the OC, also reported in literature [69]. This finding hints at a potential poisoning of the active phases of the OC due to contaminant mineral matter in the feedstock, as reported by Lebendig et al. [38]. The amorphous phase, which was found to "bridge" the OC particles inside the agglomerates, most certainly constitutes the melt at operation temperature. Correspondingly, amorphous phases mainly consisting of the major ash elements K, Si, Ca, and O were found to be located in between the individual OC particles in the (agglomerate) samples from K3 via SEM-EDX (more details see Section A.3 in the Supplementary Material). As illustrated in Fig. 23d, these amorphous phases are molten at operation temperature and therefore act as "glue", sticking individual OC particles together and promoting the unhindered growth of agglomerates. Non-agglomerated particles contained significantly lower amounts of amorphous phase. Here, the amount of melt was not (yet) sufficient in case of these particles to glue them together and form bigger agglomerates.

In terms of the mechanical rigidity of the agglomerated particles, investigation of the samples in the jet cup (see Section 2.4.4), confirmed the general findings made during inspection of the 1 MW $_{th}$ CLG pilot plant (i.e. agglomerates are brittle, more details see Section 3.4.1). While for the fresh ilmenite materials (Fig. 24a and b), as well as loop seal samples from K1 (Fig. 24c and d) no significant shift in PSD was visible inside the jet cup, loop seal samples from K3 (Fig. 24e and f)

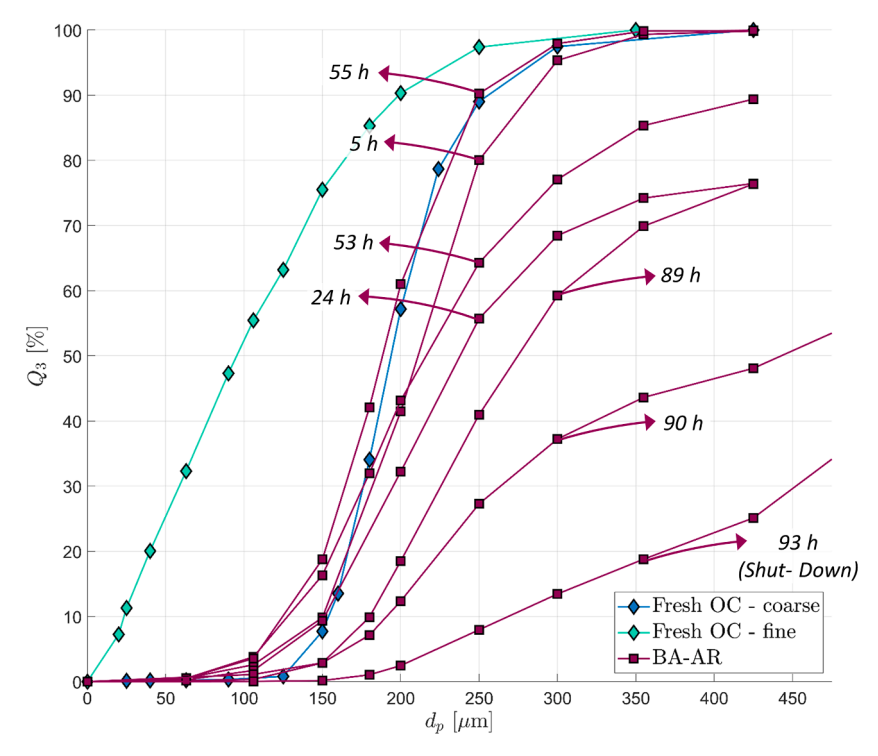


Fig. 21. Cumulative particle size distribution (PSD) of ilmenite samples collected from the AR via ash sluicing for the third test campaign (K3). PSD of fresh OC materials are given as a reference. After 9 hours of OC-aided compustion operation, chemical looping operation was initiated on 26thAugust 2022. This point in time is used as the reference time (0 h).

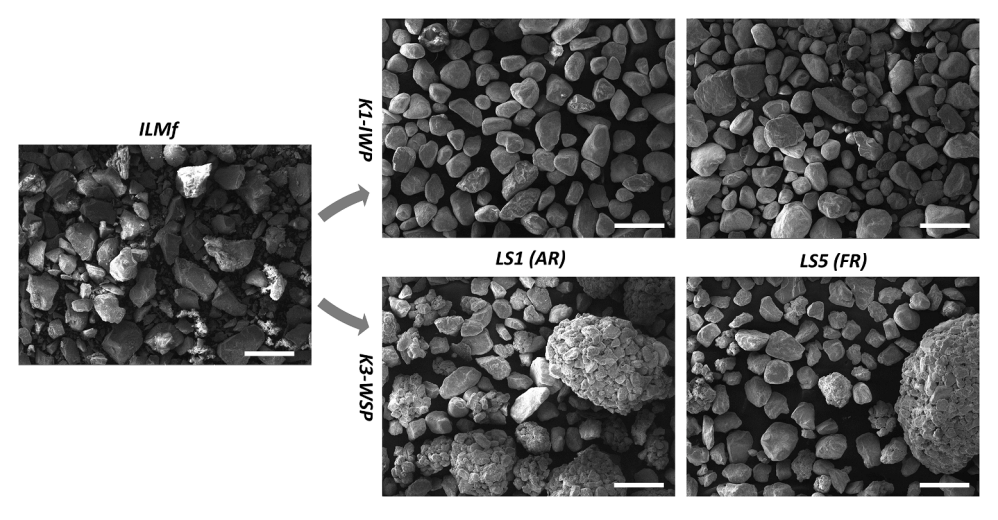


Fig. 22. SEM images of fresh ilmenite (ILMf, left), samples collected from LS1 and LS5 during K1 (top) and K3 (bottom) at 70x magnification. The white bar denotes a length of and 500 µm.

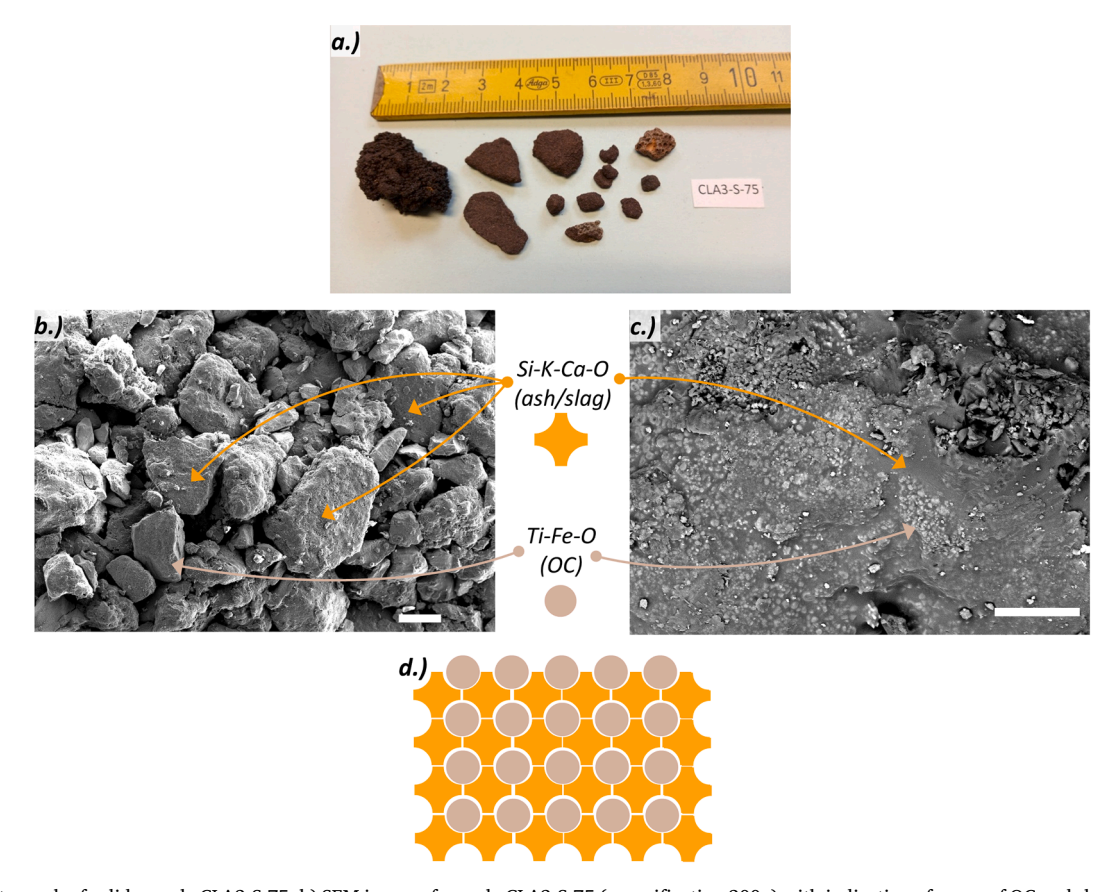


Fig. 23. a) Photograph of solid sample CLA3-S-75, b) SEM image of sample CLA3-S-75 (magnification 300x) with indication of zones of OC and slag, c) SEM image of sample CLA3-S-75 (magnification 1500x) with indication of zones of OC and slag, d) Simplified illustration of composition of agglomerates formed during 1 MW_{th} CLG operation. The white bar denotes a length of 100 μ m (b.) and 10 μ m (c.).

showed a decrease in average particle size during the attrition experiments. As visible in Fig. 24e especially larger agglomerates retrieved from LS1 broke into smaller particles inside the jet cup. This again underlines that agglomerates do not exhibit a uniform, stable structure, but rather consist of multiple particles being attached to one another via an amorphous ash phase. It can therefore be postulated that when mechanical force is applied, the agglomerates break along those binding ash "bridges" between the individual OC particles. This finding also explains why the amount of large (>1 cm) agglomerates retrieved from the AR riser was limited, as the formation of larger agglomerates are

prevented inside the turbulent gas-solid flow inside the riser. On the other hand, mechanical forces inside the lower region of the cyclone, as well as the LS1 stand-pipe were insufficient to break formed agglomerates apart, leading to a continuous agglomerate growth.

3.4.4. Summary and outlook on suggested agglomeration mitigation strategies

Based on the results from pilot testing, plant inspection, and subsequent lab-scale experiments, a mechanism explaining the occurrence of OC agglomeration in the CLG unit during K3 was derived. Here, the

origin of agglomeration was found to be the low ash melting point of the WSP ashes, which can mainly be related to their high potassium and low silica content. The molten ashes, formed mainly inside the AR where temperatures are generally higher than in the FR and where full conversion of the pellets is achieved, act as a "glue" binding OC particles together, according to the melt-induced agglomeration mechanism [66]. Consequently, the size of agglomerates increases with time, as more particles get attached to one another via an amorphous molten phase mainly composed of Calcium, Potassium, and Silicate. Moreover, the formed agglomerates were found to also be able to stick to reactor walls, especially in regions of low turbulence (e.g. stand-pipe), where the resistance to material build-up and attrition forces are low, leading to the formation of large agglomerate slabs (>15 cm).

Due to this mechanism, the average particle size inside the CLG unit increased from approx. 111 µm (fresh ilmenite) to beyond 500 µm, preventing sufficient solid circulation between AR and FR. Moreover, large, brittle slabs of agglomerates formed inside the top of the AR riser as well as the standpipe of LS1, posing another obstacle to circulating solid particles. Consequently, system hydrodynamics were significantly impaired during CLG operation with WSP, resulting in insufficient heat and oxygen transport from the AR to the FR. To counter the ensuing effects of this on the CLG process (esp. too low FR temperatures), operators first adjusted hydrodynamic boundary conditions to the maximum extent (i.e. increase in fluidization velocities) before opting to boost FR temperatures via an increase in thermal load. ¹⁸ Yet, while this approach generally leads to an increase in system temperatures for CLG operation, it resulted in a much stronger increase in AR temperatures when compared to FR temperatures for operation with the WSP due to the agglomeration-related limitations in heat and oxygen transport to the FR. 19 Consequently, the tendency towards agglomeration inside the AR increased further, thus again entailing an increase in the mean particle diameter of the OC, which ultimately led to another decrease in solid circulation rates and FR temperatures. The explained vicious cycle, leading to the extensive agglomeration behavior observed during K3, is illustrated in Fig. 25. As indicated in Fig. 25, the only way to break this cycle is the wide-ranging replacement of bed inventory with fresh OC material, resulting in a decrease in the average particle diameter and thus an increase in solid circulation rate. However, it is clear that the effect of material replacement is only of a temporary nature, as agglomeration occurs continuously.

Therefore, it can be concluded that continuous bed material replacement is required in case agglomeration occurs in considerable fashion inside the CLG unit. Depending on the extent of agglomeration occurring, the ash sluicing and make-up rates have to be adjusted by the operators, to prevent an uncontrolled increase in the average OC particle diameter with elapsed time, leading to impaired system hydrodynamics. For the 1 MWth CLG unit, the make-up rate to achieve a temporary alleviation of agglomeration-related issues was approx. three times higher than in the absence of agglomeration (K1 & K2), leading to drastically reduced OC lifetimes. An option to decrease procurement and disposal costs in a full-scale unit would be post processing of the discharged bed material from the AR and FR using a sieving apparatus, to remove agglomerates (>300 μm) and allow for a reintroduction of the remaining material via the make-up system. However, the prevention of the occurrence of agglomeration inside the CLG unit clearly would be the more preferential solution, especially when aiming to prevent the formation of larger agglomerates inside the CLG system, which can hinder material transport to significant extents.

To prevent the occurrence of agglomeration inside the CLG system for any feedstock of choice, the raw feedstock firstly has to be analyzed (esp. regarding its ash composition). Based on this analysis, an optimized biomass pre-treatment concept can be derived using a methodology comprised of simulation and experimental efforts [35]. Final analysis of the ensuing pre-treated feedstock, based on simulative and experimental investigations, can then be used to predict the risk of bed agglomeration in a CLG environment. For feedstocks with a low agglomeration tendency, additivation of substances such as CaCO3 during pelletization can be sufficient [14,48], while more problematic feedstocks require additional pre-treatment steps, such as washing, which was found to be beneficial for the removal of components tending toward ash agglomeration (e.g. potassium) [38,39,61,65]. Ultimately, this shows that technical solutions for the prevention of agglomeration inside the CLG system exist, allowing for sufficiently long OC lifetimes, regardless of the utilized raw feedstock.

4. Conclusions

In the modular 1 MW $_{th}$ pilot plant over 300 h of chemical looping operation were achieved, using three different biomasses as the feedstock. Within this study, OC samples from different locations of the 1 MW $_{th}$ pilot were analyzed regarding their morphology, composition, as well as physical and chemical properties. The main conclusions from these analyses are:

- As reported in other studies, the OC undergoes several changes during chemical looping operation, which can be related to mechanical, thermal, and chemical strains acting inside the CLG system. Here, the most important ones are iron-migration to the particle surface, an increase in particle porosity, and particle abrasion.
- For one, these changes entail particle loss in the form of fines.
 Moreover, a decrease in the oxygen transport capacity of the OC was observed, while oxygen uptake and release kinetics improve during operation due to the larger porosity of the utilized OC particles.
- In the absence of agglomeration, OC loss via particle attrition determines the lifetime of the OC inside the 1 MWth CLG system. Here, OC lifetimes of approx. 70 h were determined during operation with industrial wood pellets and pine forest residue. On the one hand, these relatively low lifetimes can be related to peculiarities of the 1 MWth system (e.g. low cyclone separation efficiencies). On the other hand, the data suggests that due to the thermal, mechanical, and chemical stresses acting in an industrial CLG setup, lower lifetimes (200–300 h) than in lab configurations (>500 h) can be realized. To further explore how OC lifetimes can be optimized, a quantification of the effect of those different stresses under industry-like conditions as well as their interplay should be carried out in future studies.
- During operation with wheat straw pellets, particle agglomeration, impeding OC circulation between AR and FR and thus preventing efficient CLG operation, was observed. The occurrence of agglomeration was related to the feedstock's ash chemistry, leading to particle agglomeration following the melt-induced agglomeration mechanism. Subsequent lab analyses showed that the agglomeration tendency of different feedstocks is predictable, allowing for the conceptualization of tailored pre-treatment concepts, facilitating the utilization of a wide array of feedstocks for CLG.

In summary, the results show that CLG operation in industry-like conditions is feasible, meaning that long-term operation in representative boundary conditions can be attained using ilmenite as the bed material. Moreover, the most important characteristics of the utilized OC particles were determined, providing value insights into the fate of the OC during CLG in semi-industrial scale. On the basis of the elucidations provided in this study, process efficiency of pilot and industrial plants can thus be optimized, thereby providing an important reference

¹⁸ When trying to increase FR temperatures in case of stable hydrodynamics (i. e. in the absence of agglomeration), an alternative to changing the solid circulation rate is increasing the thermal load of the CLG unit, which results in an overall increase in system temperatures (i.e. FR and AR temperatures increase) [58].

¹⁹ In some cases the propane load was increased instead of the thermal load of the solid feedstock, making the effect even more drastic.

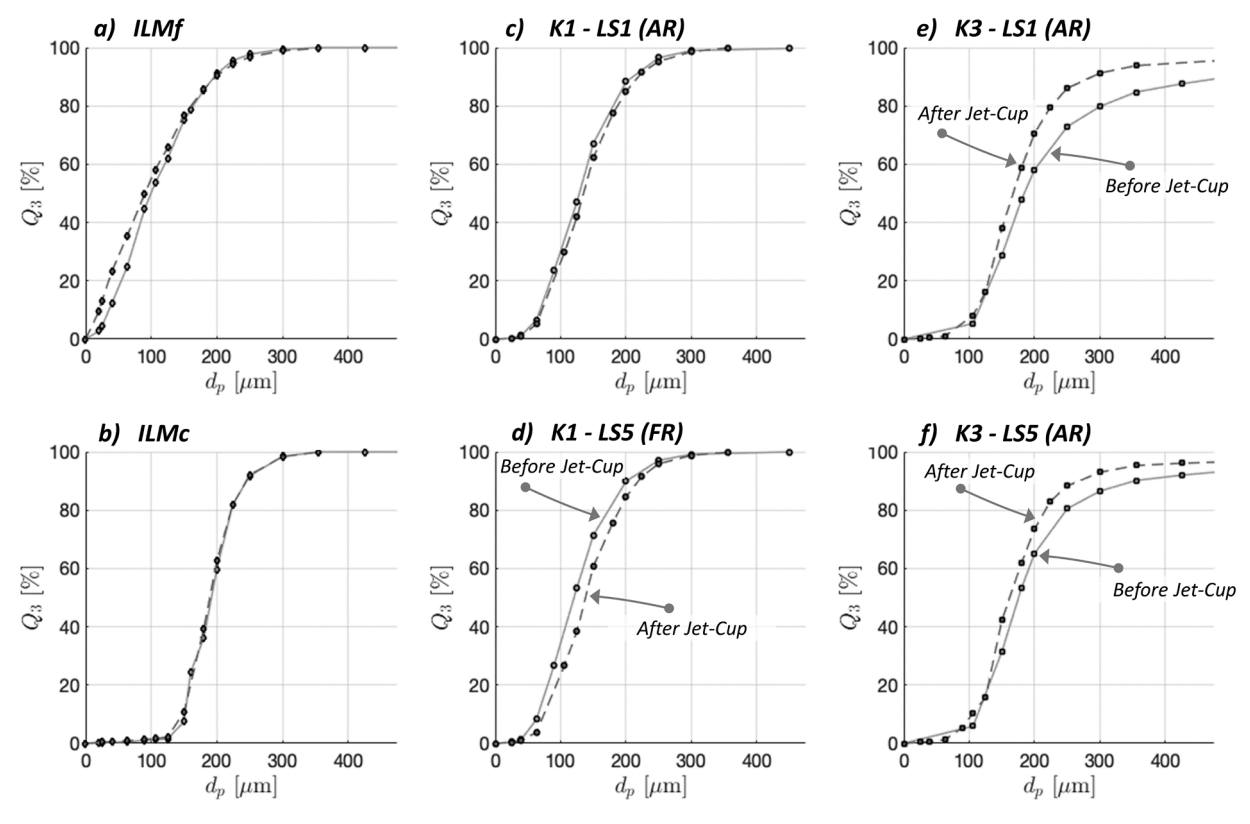


Fig. 24. PSD of OC before (-) and after (-) attrition tests in jet cup. a), b) fresh ilmenite; c), d) loop seal samples from K1; e), f) loop seal samples from K3.

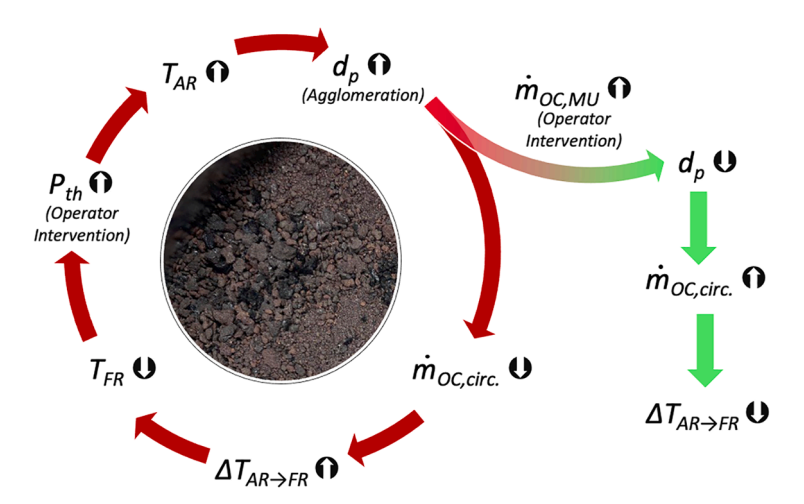


Fig. 25. Schematic illustration of proposed vicious cycle of agglomeration (red arrows), as observed during 1 MW_{th} CLG operation with WSP. Green arrows indicate the approach to break cycle during operation.

for future scale-up endeavors.

Funding

This work has received funding of the European Union's Horizon 2020-Research and Innovation Framework Programme under grant agreement No. 817841 (Chemical Looping gasification foR sustainAble production of biofuels-CLARA).

The content of this work reflects only the author's view, and the European Commission is not responsible for any use that may be made of

the information it contains.

CRediT authorship contribution statement

Paul Dieringer: Conceptualization, Methodology, Investigation, Data curation, Writing – original draft, Visualization. Falko Marx: Writing – review & editing, Methodology, Investigation, Data curation. Florian Lebendig: Methodology, Investigation. Michael Müller: Methodology, Investigation, Writing – original draft, Funding acquisition. Andrea Di Giuliano: Methodology, Investigation, Writing –

original draft, Funding acquisition. **Katia Gallucci:** Methodology, Investigation, Writing – original draft, Funding acquisition. **Jochen Ströhle:** Writing – review & editing, Supervision, Project administration, Funding acquisition. **Bernd Epple:** Resources, Funding acquisition.

Declaration of Competing Interest

The authors declare that they have no known competing financial interests or personal relationships that could have appeared to influence the work reported in this paper.

Data availability

Data will be made available on request.

Acknowledgments

The authors would like to thank Aichernig Engineering GmbH, Austria for their support in the design and safety analysis of the 1 MW $_{
m th}$ CLG unit. Moreover, the authors would like to thank AB Torkapparater, Sweden for the production, storage and shipping of pine forest residue and wheat straw pellets. Lastly, the authors would like to thank Egbert Wessel, Mirko Ziegner, Marvin Jost, Levent Aytemiz, and Niklas Engering for their support in lab analysis of the OC samples.

Supplementary materials

Supplementary material associated with this article can be found, in the online version, at doi:10.1016/j.jaecs.2023.100227.

References

- [1] World Meteorological Organization (WMO). WMO global annual to decadal climate update (target years: 2023-2027). World Meteorological Organization (WMO); 2023 [Online]. Available: https://library.wmo.int/index.php? lvl=notice_display&id=22272#.ZG5HPS210Wo.
- [2] Horowitz CA. Paris agreement. Int Leg Mater 2016;55(4):740–55. https://doi.org/ 10.1017/S0020782900004253.
- [3] European Environmental Agency (EEA), "Greenhouse gas emissions from transport in Europe," EEA Indicators. https://www.eea.europa.eu/ims/greenhouse-gas-emiss ions-from-transport (accessed Mar. 10, 2023).
- [4] International Energy Agency (IEA). Global electric vehicle outlook 2022. 2022.
- [5] Directive (EU) 2018/2001 of the European Parliament and of the Council of 11 December 2018 - on the promotion of the use of energy from renewable sources. Off J Eur Union 2018:128.
- [6] Atsonios K, Nesiadis A, Detsios N, Koutita K, Nikolopoulos N, Grammelis P. Review on dynamic process modeling of gasification based biorefineries and bio-based heat & power plants. Fuel Process Technol 2020;197:106188. https://doi.org/10.1016/ i.fuproc.2019.106188.
- [7] Roshan Kumar T, Mattisson T, Rydén M, Stenberg V. Process analysis of chemical looping gasification of biomass for Fischer–Tropsch crude production with netnegative CO₂ emissions: part 1. Energy Fuel 2022. https://doi.org/10.1021/acs. energyfuels.2c00819. acs.energyfuels.2c00819.
- [8] Higman C. Gasification. Combustion engineering issues for solid fuel systems. Elsevier; 2008. p. 423–68. https://doi.org/10.1016/B978-0-12-373611-6.00011-2.
- [9] Langner E, Kaltenmorgen J, Heinze C, Ströhle J, Epple B. Fluidized bed gasification of solid recovered fuels in a 500 kWth pilot plant. Fuel 2023;344:127901. https://doi.org/10.1016/j.fuel.2023.127901.
- [10] Nguyen NM, Alobaid F, Dieringer P, Epple B. Biomass-based chemical looping gasification: overview and recent developments. Appl Sci 2021;11(15):7069. https://doi.org/10.3390/app11157069.
- [11] Condori O, García-Labiano F, de Diego LF, Izquierdo MT, Abad A, Adánez J. Biomass chemical looping gasification for syngas production using LD Slag as oxygen carrier in a 1.5 kWth unit. Fuel Process Technol 2021;222:106963. https://doi.org/10.1016/j.fuproc.2021.106963.
- [12] Hedayati A, Soleimanisalim AH, Linderholm CJ, Mattisson T, Lyngfelt A. Experimental evaluation of manganese ores for chemical looping conversion of synthetic biomass volatiles in a 300 W reactor system. J Environ Chem Eng 2021: 105112. https://doi.org/10.1016/j.jece.2021.105112.
- [13] Huang Z, et al. Biomass char direct chemical looping gasification using Nio-modified iron ore as an oxygen carrier. Energy Fuel 2014;28(1):183–91. https://doi.org/10.1021/ef401528k.
- [14] Condori O, Abad A, Izquierdo MT, de Diego LF, García-Labiano F, Adánez J. Assessment of the chemical looping gasification of wheat straw pellets at the 20 kWth scale. Fuel 2023;344:128059. https://doi.org/10.1016/j.fuel.2023.128059.

- [15] Huseyin S, Wei G, Li H, He F, Huang Z. Chemical-looping gasification of biomass in a 10 kWth interconnected fluidized bed reactor using Fe₂O₃/Al₂O₃ oxygen carrier. J Fuel Chem Technol 2014;42(8):922–31. https://doi.org/10.1016/S1872-5813 (14)60030-6
- [16] Ge H, Guo W, Shen L, Song T, Xiao J. Biomass gasification using chemical looping in a 25 kW th reactor with natural hematite as oxygen carrier. Chem Eng J 2016; 286:174–83. https://doi.org/10.1016/j.cej.2015.10.092.
- [17] Hilz J, Helbig M, Haaf M, Daikeler A, Ströhle J, Epple B. Investigation of the fuel influence on the carbonate looping process in 1 MWth scale. Fuel Process Technol 2018;169:170–7. https://doi.org/10.1016/j.fuproc.2017.09.016.
- [18] Hilz J, Helbig M, Haaf M, Daikeler A, Ströhle J, Epple B. Long-term pilot testing of the carbonate looping process in 1 MWth scale. Fuel 2017;210:892–9. https://doi. org/10.1016/j.fuel.2017.08.105.
- [19] Ohlemüller P, Ströhle J, Epple B. Chemical looping combustion of hard coal and torrefied biomass in a 1 MWth pilot plant. Int J Greenhouse Gas Control 2017;65: 149–59. https://doi.org/10.1016/j.ijggc.2017.08.013.
- [20] Ohlemüller P, Busch J-P, Reitz M, Ströhle J, Epple B. Chemical-looping combustion of hard coal: autothermal operation of a 1 MWth pilot plant. J Energy Res Technol 2016;138(4):042203. https://doi.org/10.1115/1.4032357.
- [21] Heinze C, May J, Langner E, Ströhle J, Epple B. High temperature Winkler gasification of Rhenish lignite in an optimized 500 kWth pilot plant. Fuel 2023; 333:126289. https://doi.org/10.1016/j.fuel.2022.126289.
- [22] Marx F, Dieringer P, Ströhle J, Epple B. Design of a 1 MWth pilot plant for chemical looping gasification of biogenic residues. Energies 2021;14(9):2581. https://doi. org/10.3390/en14092581.
- [23] Johansson M, Mattisson T, Lyngfelt A. Comparison of oxygen carriers for chemical-looping combustion. Therm sci 2006;10(3):93–107. https://doi.org/10.2298/TSCI0603093J.
- [24] Adanez J, Abad A, Garcia-Labiano F, Gayan P, de Diego LF. Progress in chemical-looping combustion and reforming technologies. Prog Energy Combust Sci 2012;38 (2):215–82. https://doi.org/10.1016/j.pecs.2011.09.001.
- [25] Leion H, Lyngfelt A, Johansson M, Jerndal E, Mattisson T. The use of ilmenite as an oxygen carrier in chemical-looping combustion. Chem Eng Res Des 2008;86(9): 1017–26. https://doi.org/10.1016/j.cherd.2008.03.019.
- [26] Cuadrat A, Abad A, Adánez J, de Diego LF, García-Labiano F, Gayán P. Behavior of ilmenite as oxygen carrier in chemical-looping combustion. Fuel Process Technol 2012;94(1):101–12. https://doi.org/10.1016/j.fuproc.2011.10.020.
- [27] Adánez J, Cuadrat A, Abad A, Gayán P, de Diego LF, García-Labiano F. Ilmenite activation during consecutive redox cycles in chemical-looping combustion. Energy Fuels 2010;24(2):1402–13. https://doi.org/10.1021/ef900856d.
- [28] Nelson T, Van Der Watt JG, Laudal D, Feilen H, Mann M, Srinivasachar S. Reactive jet and cyclonic attrition analysis of ilmenite in chemical looping combustion systems. Int J Greenh Gas Control 2019;91:102837. https://doi.org/10.1016/j. jigec.2019.102837.
- [29] Condori O, García-Labiano F, de Diego LF, Izquierdo MT, Abad A, Adánez J. Biomass chemical looping gasification for syngas production using ilmenite as oxygen carrier in a 1.5 kWth unit. Chem Eng J 2021;405:126679. https://doi.org/ 10.1016/j.cej.2020.126679
- [30] Wei G, He F, Huang Z, Zheng A, Zhao K, Li H. Continuous operation of a 10 kW_{th} chemical looping integrated fluidized bed reactor for gasifying biomass using an iron-based oxygen carrier. Energy Fuel 2015;29(1):233–41. https://doi.org/10.1021/ef5021457.
- [31] Huang Z, et al. Chemical looping gasification of biomass char using iron ore as an oxygen carrier. Int J Hydrog Energy 2016;41(40):17871–83. https://doi.org/ 10.1016/j.ijhydene.2016.07.089.
- [32] Marx F, Dieringer P, Ströhle J, Epple B. Solid flux measurement in dual fluidized bed processes based on solid samples. Fuel 2023;341:127589. https://doi.org/ 10.1016/j fuel 2023.127589
- [33] Ströhle J, Orth M, Epple B. Chemical looping combustion of hard coal in a 1 MWth pilot plant using ilmenite as oxygen carrier. Appl Energy 2015;157:288–94. https://doi.org/10.1016/j.apenergy.2015.06.035.
- [34] Rydén M, Moldenhauer P, Lindqvist S, Mattisson T, Lyngfelt A. Measuring attrition resistance of oxygen carrier particles for chemical looping combustion with a customized jet cup. Powder Technol 2014;256:75–86. https://doi.org/10.1016/j. powter 2014 01 085
- [35] Di Giuliano A, Funcia I, Pérez-Vega R, Gil J, Gallucci K. Novel application of pretreatment and diagnostic method using dynamic pressure fluctuations to resolve and detect issues related to biogenic residue ash in chemical looping gasification. Processes 2020;8(9):1137. https://doi.org/10.3390/pr8091137.
- [36] Di Giuliano A, Malsegna B, Lucantonio S, Gallucci K. Experimental assessments of pyrolytic and fluid-dynamic interactions between pretreated residual biomasses and fluidized beds made up of oxygen carriers for chemical looping gasification. Adv Powder Technol 2023;34(5):104010. https://doi.org/10.1016/j. apt.2023.104010.
- [37] Di Giuliano A, Lucantonio S, Malsegna B, Gallucci K. Pretreated residual biomasses in fluidized beds for chemical looping gasification: experimental devolatilizations and characterization of ashes behavior. Bioresour Technol 2022;345:126514. https://doi.org/10.1016/j.biortech.2021.126514.
- [38] Lebendig F, Funcia I, Pérez-Vega R, Müller M. Investigations on the effect of pretreatment of Wheat Straw on ash-related issues in chemical looping gasification (CLG) in comparison with woody biomass. Energies 2022;15(9):3422. https://doi. org/10.3390/en15093422.
- [39] Lebendig F, Müller M. Effect of pre-treatment of herbaceous feedstocks on behavior of inorganic constituents under chemical looping gasification (CLG) conditions. Green Chem 2022;24(24):9643–58. https://doi.org/10.1039/D2GC02906E.

- [40] Lyngfelt A, Thunman H. Construction and 100 h of operational experience of A 10-kW chemical-looping combustor. Carbon dioxide capture for storage in deep geologic formations. Elsevier; 2005. p. 625–45. https://doi.org/10.1016/B978-008044570-0/50122-7.
- [41] L.-S. Fan, "Chemical looping systems for fossil energy conversions," p. 437.
- [42] Marinuc M, Rus F. The effect of particle size and input velocity on cyclone separation process. Bull Transilv Univ Bras II: For Wood Ind Agric Food Eng 2011: 117, 22
- [43] Wang H. Study on separation efficiency of cyclone separator for 75t/h circulating fluidized bed boiler. IOP Conf Ser: Mater Sci Eng 2020;721(1):012037. https://doi. org/10.1088/1757-899X/721/1/012037.
- [44] Bolhar-Nordenkampf M, et al. Scale-up of a 100kWth pilot FICFB-gasifier to a 8 MWth FICFB-gasifier demonstration plant in Güssing (Austria). In: presented at the Proc. 1st International Ukrainian Conference on Biomass For Energy; 2002.
- [45] Chung C, Qin L, Shah V, Fan L-S. Chemically and physically robust, commercially-viable iron-based composite oxygen carriers sustainable over 3000 redox cycles at high temperatures for chemical looping applications. Energy Environ Sci 2017;10 (11):2318–23. https://doi.org/10.1039/C7EE02657A.
- [46] Dieringer P, Marx F, Ströhle J, Epple B. System hydrodynamics of a 1 MWth dual circulating fluidized bed chemical looping gasifier. Energies 2023;16(15):5630. https://doi.org/10.3390/en16155630.
- [47] Markström P, Linderholm C, Lyngfelt A. Chemical-looping combustion of solid fuels – Design and operation of a 100 kW unit with bituminous coal. Int J Greenh Gas Control 2013;15:150–62. https://doi.org/10.1016/j.ijggc.2013.01.048.
- [48] Condori O, García-Labiano F, de Diego LF, Izquierdo MT, Abad A, Adánez J. Syngas production via Biomass Chemical Looping Gasification (BCLG) in a 50 kWth unit using ilmenite as oxygen carrier. In: Proceedings of the Fluidized Bed Conversion Conference 2022; 2022. p. 10.
- [49] Corcoran A, Knutsson P, Lind F, Thunman H. Comparing the structural development of sand and rock ilmenite during long-term exposure in a biomass fired 12 MWth CFB-boiler. Fuel Process Technol 2018;171:39–44. https://doi.org/ 10.1016/j.fuproc.2017.11.004.
- [50] De Diego LF, et al. Development of Cu-based oxygen carriers for chemical-looping combustion. Fuel 2004;83(13):1749–57. https://doi.org/10.1016/j. fuel.2004.03.003.
- [51] Li H, Sun Z, Tian L, Gao L, Xu Y, Cao Y. The investigation on the attrition of hematite oxygen carrier particles in a fluidization-based chemical looping system. Fuel Process Technol 2022;236:107441. https://doi.org/10.1016/j. fluore. 2022 107441
- [52] Dieringer P, Marx F, Alobaid F, Ströhle J, Epple B. Process control strategies in chemical looping gasification—a novel process for the production of biofuels allowing for net negative CO₂ emissions. Appl Sci 2020;10(12):4271. https://doi. org/10.3390/app10124271.
- [53] Kunii D, Levenspiel O. Fluidization engineering. Butterworth-Heinemann series in chemical engineering. 2 ed. Boston: Butterworth-Heinemann; 1991.
- [54] Bolhàr-Nordenkampf M, Rauch R, Bosch K, Aichernig C. Biomass CHP plant Güssing – using gasification for power generation. In: Proceeding of the 2nd Regional Conference on Energy Technology Towards a Clean Environment; 2003. p. 7.

- [55] H. Hermann, R. Reinhard, B. Klaus, K. Reinhard, and A. Christian, "Biomass CHP plant Güssing – a success story," p. 13.
- [56] Gogulancea V, et al. Technoeconomic and environmental assessment of biomass chemical looping gasification for advanced biofuel production. Int J Energy Res 2023;2023:1–17. https://doi.org/10.1155/2023/6101270.
- [57] Samprón I, de Diego LF, García-Labiano F, Izquierdo MT. Optimization of synthesis gas production in the biomass chemical looping gasification process operating under auto-thermal conditions. Energy 2021;226:120317. https://doi.org/ 10.1016/j.energy.2021.120317.
- [58] Dieringer P, Marx F, Michel B, Ströhle J, Epple B. Design and control concept of a 1 MWth chemical looping gasifier allowing for efficient autothermal syngas production. Int J Greenh Gas Control 2023;127:103929. https://doi.org/10.1016/ i.iigec.2023.103929.
- [59] Abad A, Adánez J, Cuadrat A, García-Labiano F, Gayán P, de Diego LF. Kinetics of redox reactions of ilmenite for chemical-looping combustion. Chem Eng Sci 2011; 66(4):689–702. https://doi.org/10.1016/j.ces.2010.11.010.
- [60] Abad A, Adánez J, García-Labiano F, de Diego LF, Gayán P, Celaya J. Mapping of the range of operational conditions for Cu-, Fe-, and Ni-based oxygen carriers in chemical-looping combustion. Chem Eng Sci 2007;62(1–2):533–49. https://doi. org/10.1016/j.ces.2006.09.019.
- [61] Miao Z, Jiang E, Hu Z. Review of agglomeration in biomass chemical looping technology. Fuel 2022;309:122199. https://doi.org/10.1016/j.fuel.2021.122199.
- [62] Lindström E, Öhman M, Backman R, Boström D. Influence of sand contamination on slag formation during combustion of wood derived fuels. Energy Fuels 2008;22 (4):2216–20. https://doi.org/10.1021/ef700772q.
- [63] Mlonka-Medrala A, Magdziarz A, Gajek M, Nowińska K, Nowak W. Alkali metals association in biomass and their impact on ash melting behaviour. Fuel 2020;261: 116421. https://doi.org/10.1016/j.fuel.2019.116421.
- [64] Bénoni D, Briens CL, Baron T, Duchesne E, Knowlton TM. A procedure to determine particle agglomeration in a fluidized bed and its effect on entrainment. Powder Technol 1994;78(1):33–42. https://doi.org/10.1016/0032-5910(93)02780-E.
- [65] Lucantonio S, Di Giuliano A, Gallucci K. Influences of the pretreatments of residual biomass on gasification processes: experimental devolatilizations study in a fluidized bed. Appl Sci 2021;11(12):5722. https://doi.org/10.3390/app11125722.
- [66] Morris JD, Daood SS, Chilton S, Nimmo W. Mechanisms and mitigation of agglomeration during fluidized bed combustion of biomass: A review. Fuel 2018; 230:452–73. https://doi.org/10.1016/j.fuel.2018.04.098.
- [67] de Diego LF, García-Labiano F, Gayán P, Celaya J, Palacios JM, Adánez J. Operation of a 10kWth chemical-looping combustor during 200 h with a CuO-Al₂O₃ oxygen carrier. Fuel 2007;86(7–8):1036–45. https://doi.org/10.1016/ i.fuel.2006.10.004.
- [68] Huang Z, et al. Synthesis gas production through biomass direct chemical looping conversion with natural hematite as an oxygen carrier. Bioresour Technol 2013; 140:138–45. https://doi.org/10.1016/j.biortech.2013.04.055.
- [69] Öhman M, Nordin A, Skrifvars B-J, Backman R, Hupa M. Bed agglomeration characteristics during fluidized bed combustion of biomass fuels. Energy Fuels 2000;14(1):169–78. https://doi.org/10.1021/ef990107b.